Oligopaint DNA FISH as a tool for investigating meiotic chromosome dynamics in the silkworm, *Bombyx mori*

Leah F. Rosin[1,2,*], Jose Gil Jr.[3,4], Ines A. Drinnenberg[3,4], Elissa P. Lei[1,2,*]

[1]Nuclear Organization and Gene Expression Section; [2]Laboratory of Biochemistry and Genetics, National Institute of Diabetes and Digestive and Kidney Diseases, National Institutes of Health, Bethesda, Maryland, USA; [3]Institut Curie, PSL Research University, CNRS, UMR3664, 75005 Paris, France; [4]Sorbonne Université, Institut Curie, CNRS, UMR3664, 75005 Paris, France

*Corresponding authors:

E-mail: leah.rosin@nih.gov; leielissa@niddk.nih.gov

Abstract

Accurate chromosome segregation during meiosis is essential for reproductive success. Yet, many fundamental aspects of meiosis remain unclear, including the mechanisms regulating homolog pairing across species. This gap is partially due to our inability to visualize individual chromosomes during meiosis. Here, we employ Oligopaint FISH to investigate homolog pairing and compaction of meiotic chromosomes in a classical model system, the silkworm *Bombyx mori*. Our Oligopaint design combines multiplexed barcoding with secondary oligo labeling for high flexibility and low cost. These studies illustrate that Oligopaints are highly specific in whole-mount gonads and on meiotic chromosome spreads. We show that meiotic pairing is robust in both males and female meiosis. Additionally, we show that meiotic bivalent formation in *B. mori* males is highly similar to bivalent formation in *C. elegans*, with both of these pathways ultimately resulting in the pairing of chromosome ends with non-paired ends facing the spindle pole and microtubule recruitment independent of the centromere-specifying factor CENP-A.

Author's Summary

Meiosis is the specialized cell division occurring exclusively in ovaries and testes to produce egg and sperm cells, respectively. The accurate distribution of chromosomes (the genetic material) during this process is essential to prevent infertility/sterility and developmental disorders in offspring. As researchers are specifically unable to study the mechanisms regulating meiosis in depth in humans, identifying broadly conserved aspects of meiotic chromosome segregation is essential for making accurate inferences about human biology. Here, we use a sophisticated chromosome painting approach called Oligopaints to visualize and study chromosomes during meiosis in the silkworm,

Bombyx mori. We illustrate that Oligopaints are highly specific in *B. mori* and demonstrate how Oligopaints can be used to study the dynamics of meiotic chromosomes in diverse species.

Introduction

Precise homolog pairing and unpairing during meiosis is essential for genetic recombination and accurate chromosome segregation. Errors in chromosome segregation during meiosis can lead to reduced fertility, miscarriages, or chromosomal disorders in progeny, such as Down Syndrome or Turner Syndrome (1). Decades of research has gone into characterizing the synaptonemal complex (SC), a proteinaceous structure that holds homologs together during meiotic prophase and is conserved across species (2,3). Yet how homologs find each other and come together in 3D space is still poorly understood. One of the main reasons that homolog pairing has remained such an enigma is the lack of cytological tools available for assaying chromosome- and locus-specific pairing dynamics during meiosis. Several recent studies have taken advantage of advances in super resolution microscopy techniques, such as Structure Illumination Microscopy (SIM) and Stochastic Optical Reconstruction Microscopy (STORM), to visualize meiotic pairing in more detail than ever before (4–9). However, these approaches have been limited to studying pairing genome-wide by fluorescently labeling elements of the SC (5,7–12) or to visualizing small genomic loci by FISH (13–16).

Recent technological innovations in the design and synthesis of specialized DNA FISH probes called Oligopaints have made visualizing whole, individual chromosomes or complex sub-chromosomal loci in meiotic cells feasible. Unlike traditional BAC-based FISH probes, Oligopaints are computationally designed based on genome sequence data (17,18). This approach allows for only unique, single copy sequences to be labeled, significantly increasing the specificity and resolution of FISH. Here, we leverage the flexibility of the Oligopaint design to add barcodes to label either whole

chromosomes or different sub-chromosomal loci using the same set of oligos, as previously described (19). This multiplexed approach allows for many different highly specific FISH probes to be generated at low cost and high throughput. Oligopaints and related oligo-based FISH approaches have previously been used for karyotype analyses or characterization of interphase chromosome dynamics in *Drosophila*, *C. elegans*, mammals, and plants (16,19–31). Recently, similar approaches have also been applied to the study of small chromosomal loci during meiosis (32,33), but Oligopaints have never before been used to characterize compaction and pairing of multiple, whole chromosomes during meiosis. Finally, Oligopaints have never been used to visualize chromosomes in Lepidoptera (moths and butterflies).

Here, we combine Oligopaint DNA FISH with one of the first model systems ever used to study meiotic chromosomes, the silkworm moth *Bombyx mori*. *B. mori* are holocentric insects, with centromeres forming all along the chromosome during mitosis (34–37). The holocentric mitotic configuration is also seen in many plants and nematodes, including *C. elegans* (38–40). However, the holocentric chromosome configuration prevents accurate biorientation of bivalents formed after recombination and is therefore incompatible with canonical meiosis (40,41). Instead, chromosomes in holocentric organisms often display “telokinetic” or “telokinetic-like” chromosomes during meiosis, where kinetochore activity is restricted toward telomere domains (42–48). In *C. elegans*, which telomere faces poleward to connect to the spindle microtubules is dictated by crossover position (42,46,49–51). A similar telokinetic mechanism for segregation meiotic chromosomes was also previously hypothesized to occur in *B. mori* (52–54) but has never before been directly observed. Furthermore, meiotic segregation in *C. elegans* occurs in the absence of the centromere-specifying factor Centromere Protein A (CENP-A) (51), and instead, microtubules either run parallel to chromosomes to facilitate segregation or directly penetrate chromosome ends (47,55). Interestingly,

CENP-A is entirely absent from the genomes of butterflies and moths (56). Yet, how moths and butterflies segregate chromosomes during meiosis in the absence of CENP-A remains to be explored.

Unlike *B. mori* spermatogenesis, which has been reported to support crossovers and canonical pairing, oogenesis in *B. mori* is quite unconventional. Chiasmata are not observed in female meiosis in silkworms and furthermore, the central elements of the SC break down just after pachytene (one of the sub-stages of meiotic prophase I) and the lateral elements of the SC are thought to be completely remodeled to form masses of "elimination chromatin" between the two homologs (54,57–59). This "elimination chromatin" or "modified SC" is reported to be over one micron in width, thereby ultimately undoing end-to-end homolog pairing while still holding homologs together until anaphase I (59). Thus, pairing along the entire length of the chromosomes is not expected after pachytene.

Our studies here illustrate that Oligopaints are robust and specific in germline cells and that Oligopaints can be used to visualize chromosomes even in unconventional model systems with draft genomes. Our FISH-based assays clearly demonstrate that telomeric regions face poleward and likely act as localized kinetochores during *B. mori* male meiosis and that both telomeres on any given chromosome harbor the ability to act as local kinetochores. Additionally, our data suggest that in female meiosis, homologs remain tightly paired throughout meiotic prophase I despite modifications to the SC. Overall, we provide the first extensive characterization of whole and sub-chromosome dynamics in meiosis in any species, thereby pioneering the use of Oligopaints as a tool for studying meiotic pairing and progression.

Results

Bombyx mori Oligopaint design

To visualize chromosomes in the silkworm, *B. mori*, we designed and generated Oligopaint libraries targeting six of the 27 autosomes and the Z sex chromosome. These Oligopaint libraries were designed using the Oligominer pipeline (18,60) based on the updated 2019 silkworm genome assembly (61). Oligos were designed with 80 base pairs of homology and map to the genome only once (therefore only labeling unique, single copy sequences). This yielded a maximum probe density of approximately 3 oligos per kilobase (kb) of DNA. For most chromosomes, this density was then reduced to 1 or 1.5 probes per kb (see Table 1), a probe density that has been previously shown to be sufficient for whole chromosome paints (Rosin et al 2018). The resulting oligos are fairly evenly distributed along each chromosome, with gaps in regions where repetitive sequences are more abundant (Figure 1A-C). These oligo libraries were then multiplexed as previously described (19) with one or more barcode sequences to allow for the amplification of individual chromosomes, sub-chromosomal stripes, and/or active and inactive chromatin domains (Tables 1-5; Figure 1B-C, Figure S1). In total, the libraries consisted of 191,536 oligos (designated as “primary oligos”) up to 160 bp in length, which includes the 80 bp of homology, up to two unique 20 bp sub-chromosomal barcodes, and two 20 bp whole chromosome universal barcodes (Figure 1D). During the PCR amplification steps, secondary oligo binding sites are added to the primary oligos, to which fluorescently labeled secondary oligos will anneal during the FISH protocol (Figure 1E; (21,30)). This method allows for increased flexibility when combining probes for multi-channel imaging. Together, this multiplexed probe design combined with secondary oligo labeling both increases the efficiency of Oligopaint synthesis and reduces the cost of Oligopaints.

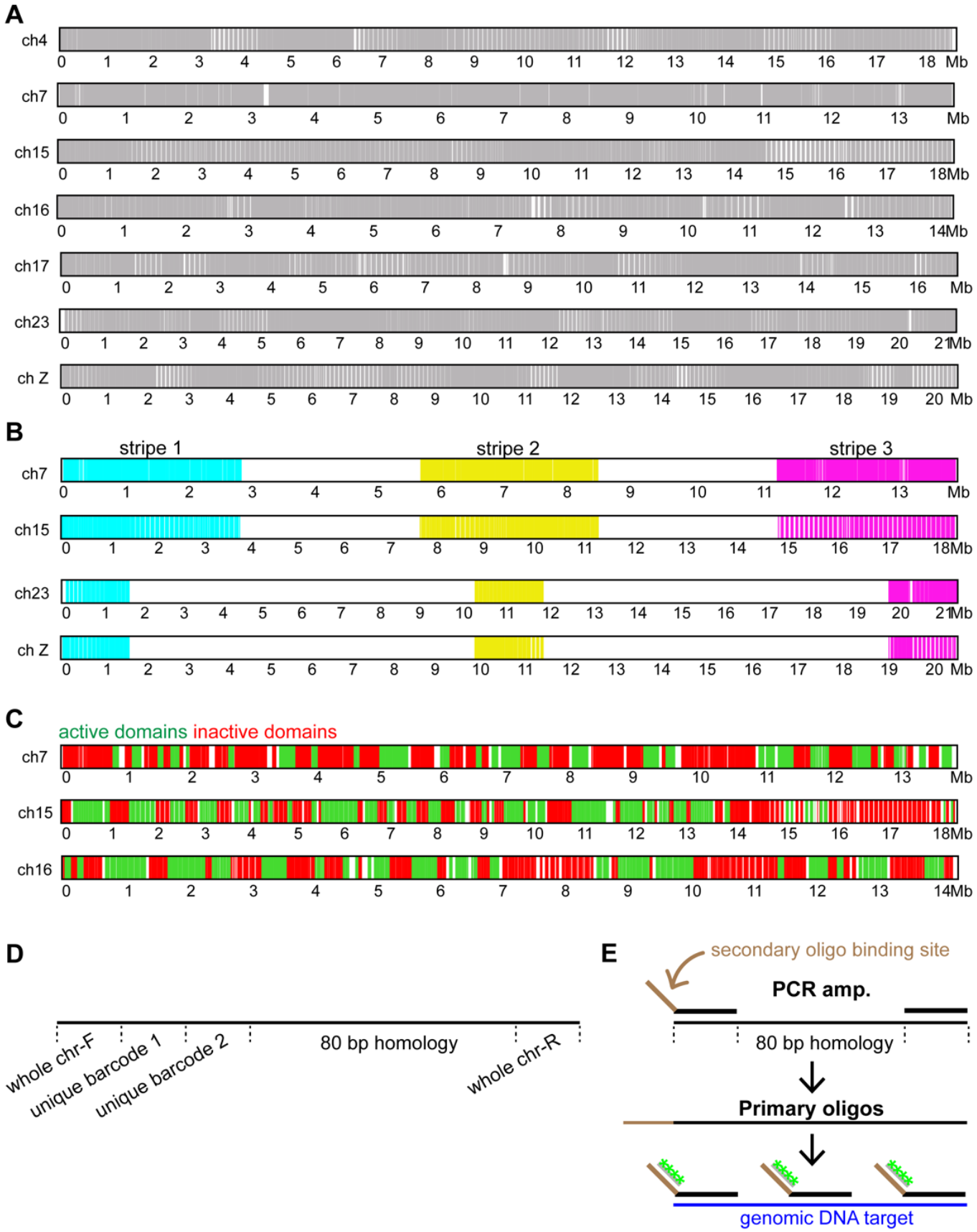

Figure 1. *B. mori* Oligopaint design.
A-C) Schematic of Oligopaints in *B. mori*. Whole chromosome Oligopaints are shown in A, stripe Oligopaints in B, and active/inactive Oligopaints in C. White regions indicate the absence of oligos (A) or regions not labeled by the respective barcode indices (B, C). D) Schematic of primary probe design, showing whole chromosome barcodes and two unique barcodes (for stripes or active/inactive domains). E) Schematic for Oligopaint DNA FISH assay with labeled secondary oligos. First, ordered oligos are amplified with primers containing barcode of interest and secondary oligo binding site, generating primary oligos. Primary oligos are then annealed to DNA and labeled with secondary oligos (shown in green).

B. mori Oligopaints are highly specific

As the *B. mori* genome used to design the Oligopaints is in a semi-draft state (assembled into chromosomes but still with many unmapped contigs), we first tested the specificity of our *B. mori* chromosome paints using karyotype analysis. To this end, meiotic chromosome spreads were prepared from late 4th or early 5th larval testes and ovaries. As silkmoths have a very short adult lifespan (only 5-7 days), meiosis begins early in the larval stages (62). Due to the small, holocentric nature of silkworm chromosomes, mitotic chromosomes are small and highly compact, while chromosomes in meiotic prophase I (pachytene sub-stage; Figure 2A; reviewed in (63)) are more linear due to synapsis (Figure S2)(64), making meiotic chromosomes better suited for our karyotype analyses. Since homologs are paired during most sub-stages of meiotic prophase I (Figure 2A), the expectation was a single fluorescence signal per chromosome. A detailed description of our pachytene chromosome spread protocol used for Oligopaint FISH can be found in the Materials and Methods.

Using our whole chromosome paints, three chromosomes at a time were labeled on pachytene chromosome spreads from testes and ovaries. This, indeed, illustrated singular and distinct fluorescence signals for each tested chromosome during pachytene (Figure 2B-2E, 2F, and 2I). In our larval testes squashes, we also were able to identify cells in early meiotic prophase I before pairing has completely occurred (leptotene/zygotene; (Figure 2F, 2H). Interestingly, a wide variety of partially paired chromosome configurations were observed at this stage, many of which contain large

chromosome loops (Figure S3A). Furthermore, we noticed that all chromosomes do not pair simultaneously, as many cells harbor some paired and some unpaired chromosomes (Figure S3B).

In addition to early prophase, cells in late prophase (post-pachytene) could also be distinguished. In our testes squashes, we identified cells with more condensed, paired chromosomes as being in diplotene/diakinesis (also known as the diffuse stage based on chromatin morphology, Figure 2F, 2J). Furthermore, we were able to identify cells in which chromosomal bivalents are compacted and aligned at the metaphase plate (metaphase I, Figure 2G, 2K). Finally, we observed somatic cells in our testes squahses harboring two distinct fluorescence signals per chromosomes, indicating that homologs are unpaired in the majority of somatic cells in *B. mori* (Figure S4).

In larval ovary squashes, we were able to identify linear, paired pachytene chromosomes (Figure 2E). Additionally, post-pachytene nurse cells could be identified by their unpaired, condensed chromosomes (Figure S5; (58)). Finally, mitotic cells are also present in the gonads, and thus were also used as additional validation of our probe specificity (Figure 2L, S2, and S6). Interestingly, when we tested these same whole chromosome paints on mitotic chromosome spreads from a *B. mori* ovary-derived cell line, BmN4, we found that our probes partially labeled multiple chromosomes, suggesting that the karyotype in these cells has undergone dramatic rearrangements compared to the genome-derived strain (Figure S7). Together, these data not only illustrate that our Oligopaint libraries are specific but also act as a validation for the *B. mori* genome assembly.

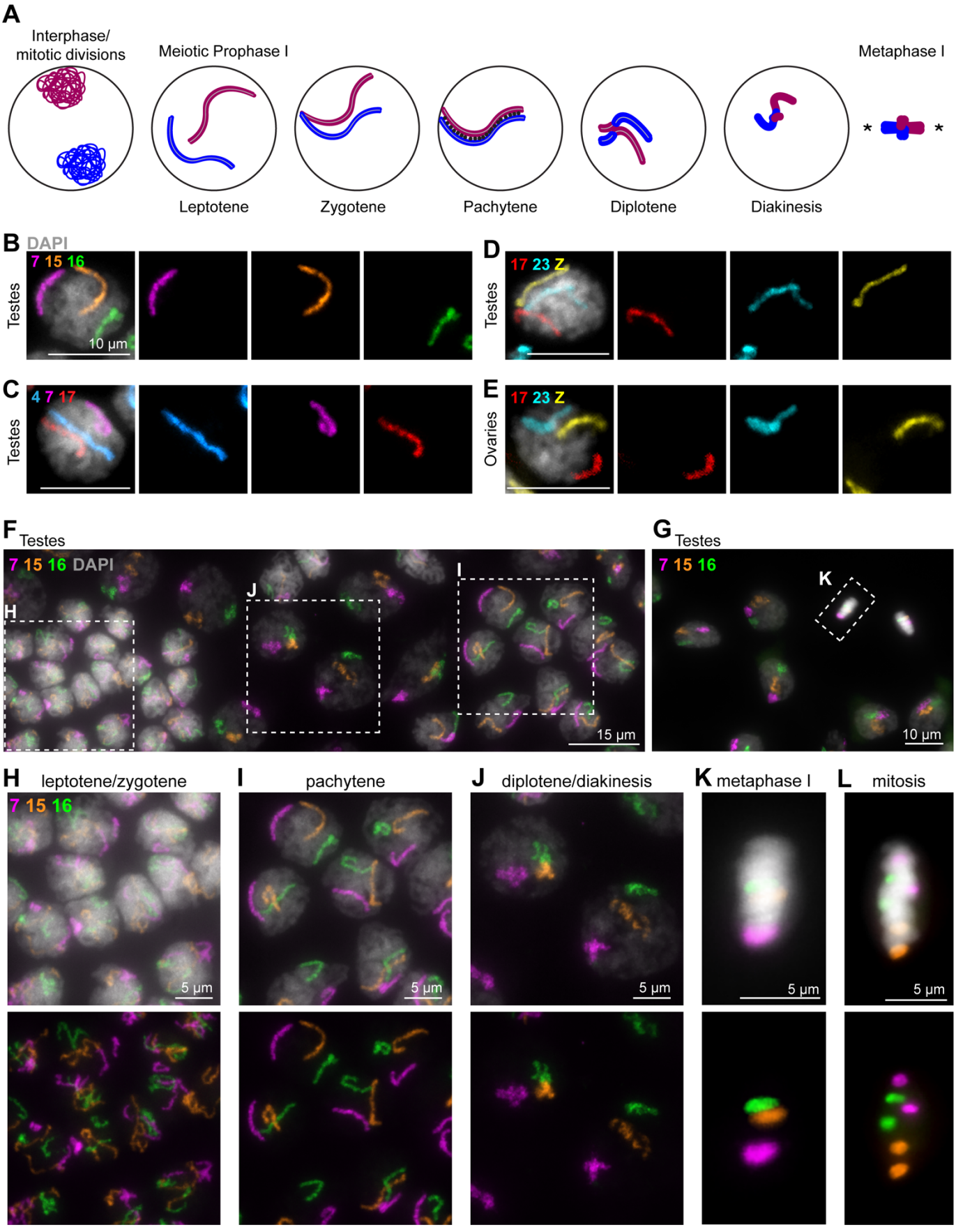

Figure 2. Whole chromosome Oligopaints in *B. mori* 5th instar germline squashes.
A) Schematic of early meiosis I (prophase I and metaphase I). One pair of homologous chromosomes is shown (red = paternal; blue = maternal). Prophase I is typically subdivided into five distinct stages: leptotene, zygotene, pachytene, diplotene, and diakinesis. Briefly: *in leptotene, replicated chromosomes are reorganized and compacted into a linear scaffold structure. In zygotene, synapsis begins between the homologous chromosomes. In pachytene, synapsis is complete (black dots represent the synaptonemal complex holding the homologs together). This is also when crossing over can occur. In diplotene, the homologs repulse, condense further, and the SC breaks down. The homologs remain attached via chiasma (crossovers). Finally, in diakinesis, chromosome condensation and cruciform bivalent formation is nearly complete as the cell prepares for metaphase I.* Asters in metaphase I schematic indicate the spindle poles. B-E) Pachytene cells labeled with three whole chromosome Oligopaints, as labeled. A-C, larval testes. D, larval ovary. Scale bars = 10 µm. DAPI is shown in gray. F-G) Meiotic prophase I and metaphase I (F) cells from larval testes squash with whole chromosome paints for ch7 (magenta), ch15 (orange), and ch16 (green). Boxes indicate subsequent panels as indicated. DAPI is shown in gray. H-K) Zooms from E-F, as indicated below. H) Leptotene/zygotene cells, with unpaired, decondensed chromosomes. I) Pachytene cells, with paired, linear, and relatively decondensed chromosomes. J) Diplotene/diakinesis cells, with paired, less linear and more compact chromosomes. K) Metaphase I cells, with paired homologs condensed and aligned along the metaphase plate. L) Mitotic cells from larval testes, with chromosomes condensed and aligned along the metaphase plate but with unpaired homologs.

Detection of stripe and chromatin state sub-libraries

While the specificity of our whole chromosome paints indicated that the *B. mori* genome is accurately assembled at the chromosome level, we needed to validate the intra-chromosomal genome assembly and in turn, the specificity of our sub-chromosomal paints. For this, we again turned to pachytene chromosome spreads in the male germline, where the linear nature of chromosomes allowed us to verify the linear order of our probes. We started with the stripe sub-libraries, wherein selected chromosomes were sub-divided into 5 stripes approximately 3 Mb in size, or 13 stripes approximately 1.5 Mb in size, depending on the chromosome (Table 2 and Figure 1B). Only the first, middle, and last stripes were labeled with secondary oligos to visualize three stripes along each chromosome (Figure 1B, 3A, 3B; stripe 1, 2 and 3, respectively). FISH with these stripe paints for ch15 in pachytene spreads from larval testes revealed a singular focus for each stripe, with stripes 1, 2, and 3 positioned in the predicted order along the linear chromosome (Figure 3A). This was also true for ch23 and the Z chromosome (Figure 3B-C).

To test the specificity of our transcriptionally active and inactive chromatin domain paints, we labeled all three chromosomes with this barcode index (ch7, 15, and 16) at the same time on larval testes pachytene spreads. This revealed three separate linear chromosomes with distinct banding

patterns (Figure 3D) corresponding to the respective paint schematic (Figure 1 and 3D). Together, these results indicate that the intra-chromosomal assembly for these chromosomes is highly accurate and our paints are specific for their target chromosomal domains.

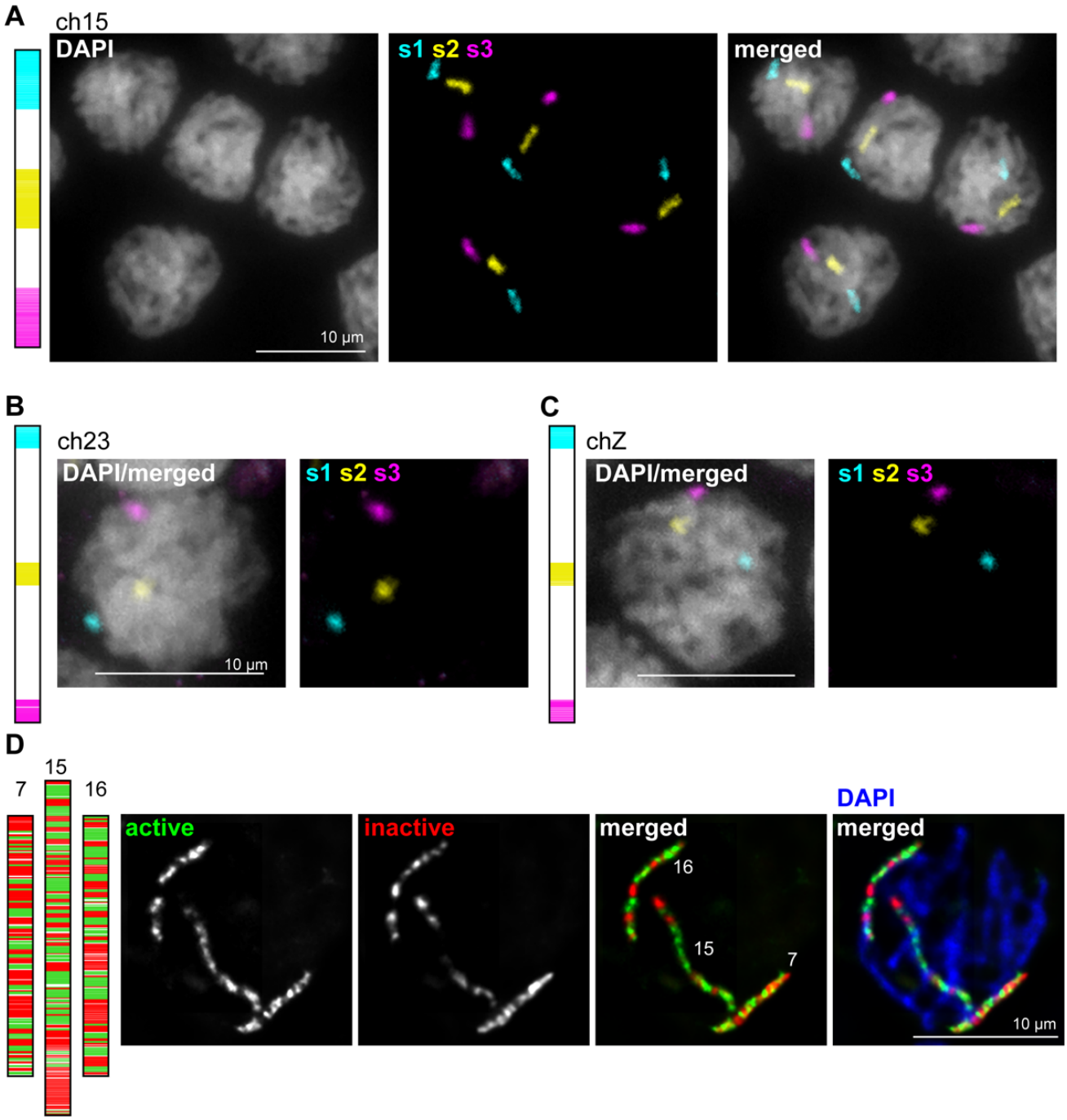

Figure 3. Stripe and active/inactive chromosome paints in *B. mori* 5th instar testes squashes.
A) Left: Schematic of stripe paints for ch15, with stripe 1 (s1) in cyan, stripe 2 (s2) in yellow, and stripe 3 (s3) in magenta. Right: Pachytene cells labeled with ch15 stripe paints. B-C) Left: Schematic of stripe paints for ch23 or chZ. Right: Representative pachytene nucleus labeled with stripe paints for ch23 or chZ. D) Left: Schematic of active/inactive paints for ch7, 15, and 16. Active domains are shown in green and inactive domains are shown in red. Right: Representative pachytene nucleus labeled with paints for all 3 chromosomes.

Telomeres face poleward at random in metaphase I bivalents in testes

In addition to identifying pachytene cells in our assays with the stripe paints in larval testes, we were able to identify cells in all stages of meiosis I up to metaphase I, as well as cells in interphase (Figure 4A). Interestingly, we noted that traditional cruciform bivalents are formed at metaphase I, and these bivalents are highly reminiscent of those seen in meiosis in the nematode *C. elegans*, with one telomere remaining paired and the other telomere facing poleward ((Figure 4B-D) reviewed in (44)). While this "telokinetic" chromosome configuration was previously hypothesized to occur in meiosis in *B. mori*, it has never before been directly observed.

We next wanted to determine if both telomeres of a chromosome can act as localized kinetochores during meiosis in *B. mori* or if one telomere preferentially faces poleward. In *C. elegans*, either telomere on any given chromosome can harbor kinetochore activity, and both do so at random depending on where crossovers form during meiotic prophase I (42,49). To test whether a similar mechanism occurs in *B. mori*, we examined metaphase I bivalents in larval testes using our stripe paints for chromosomes 15, 23, and Z. Quantification of which telomere remains paired and which telomere faces poleward (stripe 1 or stripe 3) revealed that approximately half of metaphase I cells harbor pairing in the stripe 1 domain and half harboring pairing in the stripe 3 domain for all tested chromosomes, including ch Z (Figure 4E). This finding suggests, like nematodes, *B. mori* telomere regions likely act as localized kinetochores during meiosis. Furthermore, the orientation of chromosomes in the bivalent is not pre-determined, with both telomeres having an equal probability of being either paired or facing poleward.

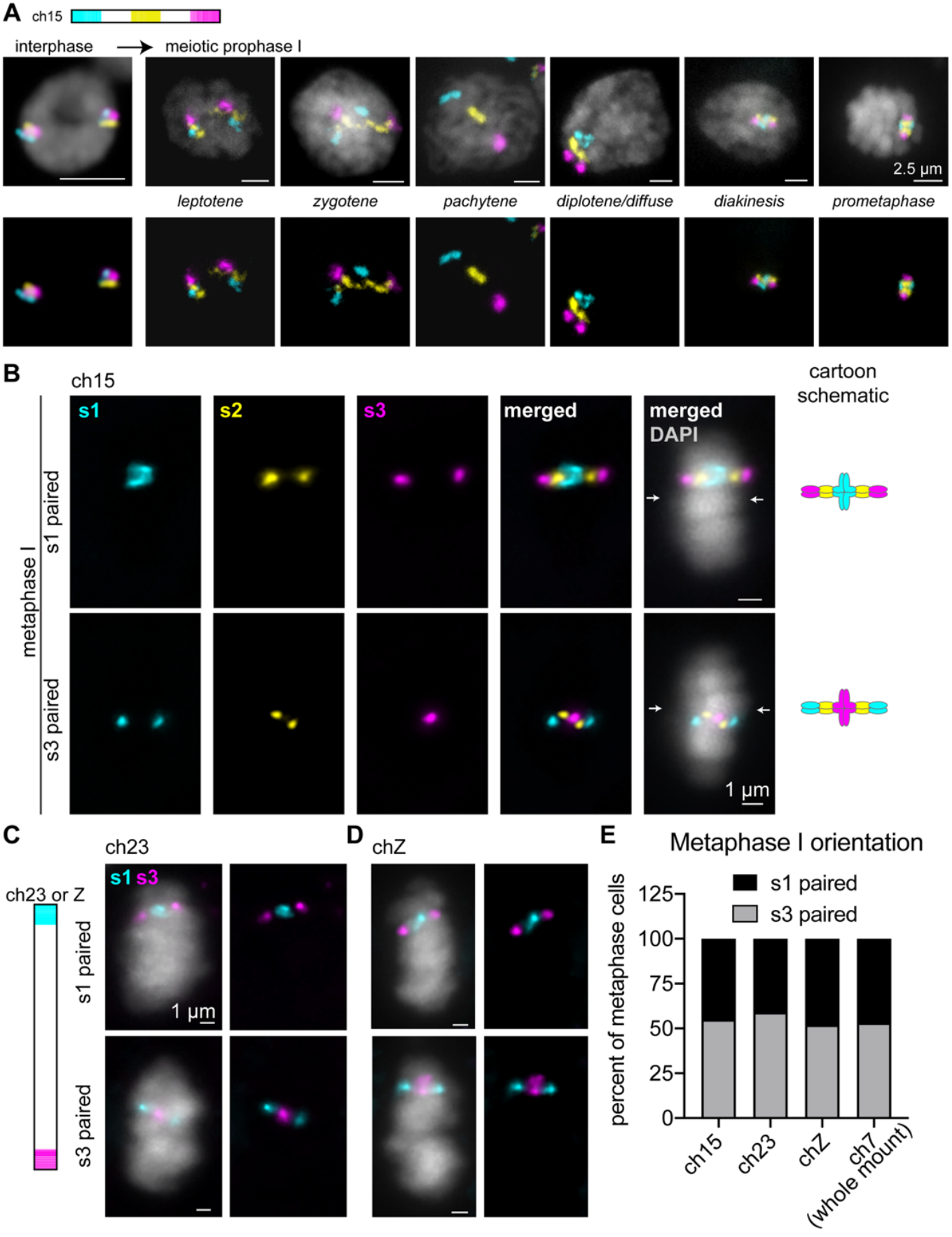

Figure 4. Analysis of pairing and metaphase I bivalent formation in 5th instar larval testes squashes.
A) Left: Schematic of stripe paints for ch15, with stripe 1 (s1) in cyan, stripe 2 (s2) in yellow, and stripe 3 (s3) in magenta. Right: representative nuclei at the designated stages labeled with ch15 stripe paints. When cells enter meiosis, chromosomes begin to decondense (leptotene) and homologs pair (zygotene). Pairing is complete by pachytene, with complete synapsis for crossing over, and chromosomes are linear. Chromosomes begin to condense for segregation in diplotene and diakinesis. DAPI is shown in gray. B) Metaphase I bivalents labeled with ch15 stripe paints. Top: bivalent with pairing in stripe 1 domain. Bottom: bivalent with pairing in stripe 3 domain. Schematics of bivalents shown on the right. C) Left: Schematic of stripe paints for ch23 or Z, showing only stripe 1 (cyan) and stripe 3 (magenta). Right: representative metaphase I cells showing pairing in the s1 domain (top) or s3 domains (bottom) for ch23. D) Representative metaphase I cells showing pairing in the s1 domain (top) or s3 domains (bottom) for chZ. E) Quantification of metaphase I orientation for ch15, 23, Z, and 7 (from whole-mount larval testes). Ch15, n=182 (45% s1 paired). Ch23, n=144 (41% s1 paired). ChZ, n=169 (48% s1 paired). Ch7, n=96 (47% s1 paired). Each FISH assay was performed on a different larva.

To further validate this finding, we repeated the experiment using chromosome 7 stripe paints in whole mount late 5th instar larval testes (Figure S8). As we predicted based on our testes squashes and previous studies (54), 5th instar larval testes harbor mitotic cells with unpaired homologs that highly resemble mitotic cells seen in whole-mount embryos (Figure 5A-B; Figure S9) and primary spermatocytes at all stages of meiosis I (Figure 5A-D). Interestingly, *B. mori* and other Lepidopteran insects utilize two distinct spermatogenic pathways, ultimately resulting in apyrene (without nuclei) and eupyrene (with nuclei) sperm (65–71). In whole-mount testes, we were clearly able to identify eupyrene secondary spermatocyte bundles (Figure 5C-3) and mature eupyrene sperm (Figures S10 and S11). Additionally, we identified secondary spermatocyte bundles appearing to be apyrene-destined, where some cells have no DNA and the FISH signal is instead diffuse in the cytoplasm, suggesting that the cells in these bundles are beginning the process of nuclear degradation (Figure 5C-4). Importantly, quantification of metaphase I bivalent formation in whole mount testes was completely in agreement with our findings from squashes, showing ch7 stripe 1 paired in 46.9% of cells and ch7 stripe 3 paired in 53.1% (Figure 4E). Together, these findings suggest that *B. mori* chromosomes form traditional bivalent structures at metaphase I with localized centromere activity restricted to one telomeric region at random.

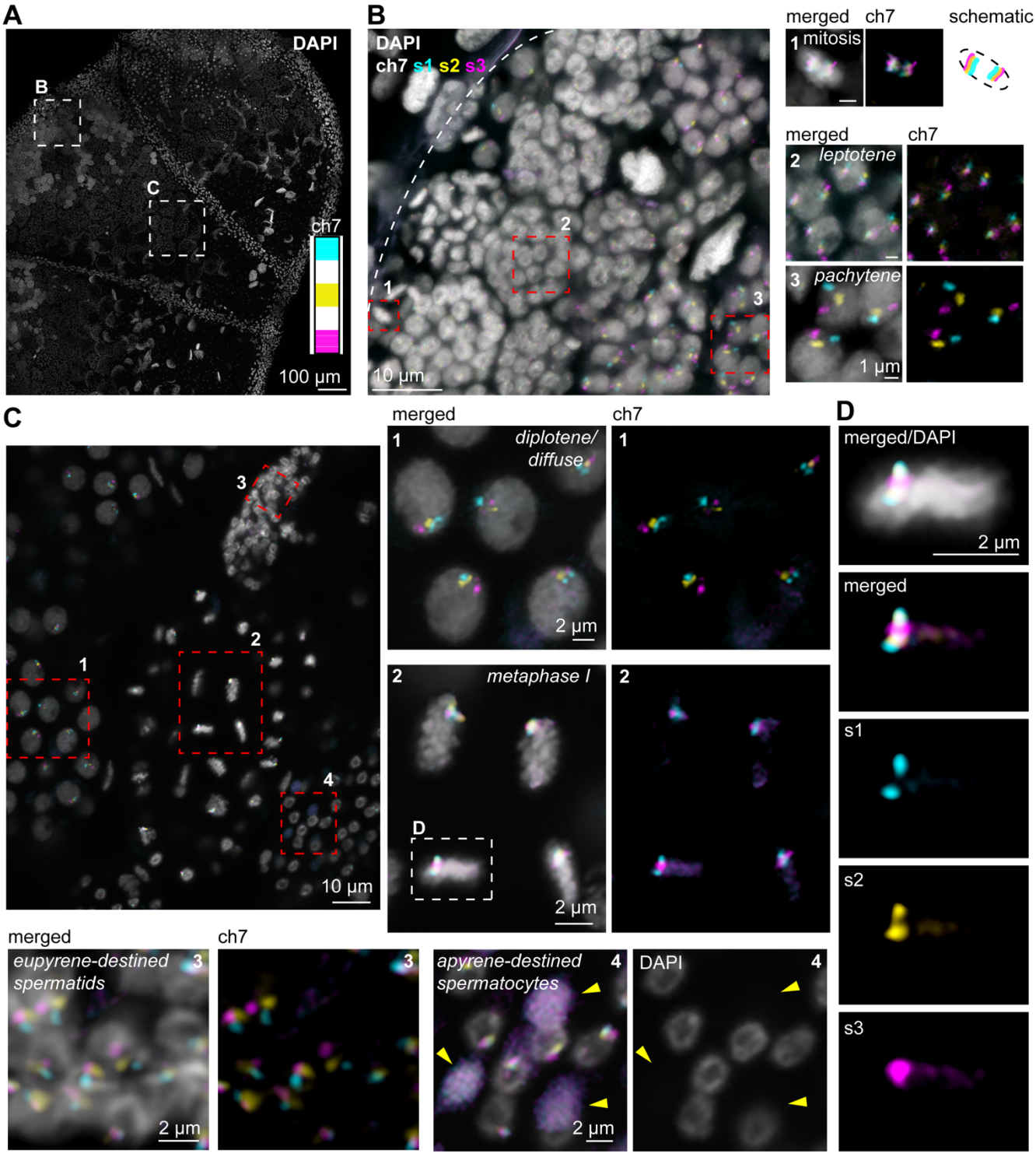

Figure 5. FISH with stripe chromosome paints in whole mount 5th instar larval testes.
A) 5th instar larval testis stained with DAPI. Boxes indicate subsequent panels as indicated. Inset: ch7 stripe paints used in B-D. B) Zoom of mitotic and pachytene region of larval testes as shown in A, labeled with ch7 stripe paints. Red boxes indicate zooms shown to the right. 1) mitotic cells – chromosomes condensed, homologs unpaired, and aligned at the metaphase plate. Note how chromosomes are compacted perpendicular to the metaphase plate. 2) leptotene cells, chromosomes are slightly decondensed and homologs are unpaired. 3) pachytene cells, chromosomes are paired head-to-tail and linear. C) Zoom of late prophase/metaphase I region of larval testis as shown in A, labeled with ch7 stripe paints. Red boxes indicate zooms shown to the right and below. 1) diplotene cells (diffuse stage), chromosomes are still paired and beginning to condense. Left: merged with DAPI in gray. Right: ch7 stripe 1 in cyan, stripe 2 in yellow, and stripe 3 in

magenta. 2) metaphase I cells labeled with ch7 stripe paints. White box indicates zoom shown in D. Left: merged with DAPI in gray. Right: stripe 1 (cyan) and stripe 3 (magenta) paints. 3) eupyrene-destined secondary spermatocyte bundle. Left: merged ch7 stripe paints with DAPI in gray. Right: ch7 stripe paints, stripe 1 (cyan) and stripe 3 (magenta). 4) apyrene-destined secondary spermatocyte bundle. Left: merged ch7 stripe paints with DAPI in gray. Right: DAPI. Yellow arrowheads indicate spermatocytes that have already undergone nuclear degradation. Scale bar = 2 um for all panels 1-4. D) Zoom of metaphase I cell indicated in C-2. Top: merged with DAPI in gray. Bottom: ch7 stripe 1 (cyan), stripe 2 (yellow), and stripe 3 (magenta) paints. Bivalent pairing is in stripe 3 domain in this cell. Note: zoomed fields for all panels may display a slightly different Z position than the larger field views.

Chromosome-wide homolog pairing is persistent in *B. mori* female larval ovaries

In contrast to what we and others have observed in *B. mori* males, homolog pairing in *B. mori* females is reported to be unconventional, without chiasma formation and with the SC transforming into "elimination chromatin" over one micron in width (54,57–59). Despite these previous observations, we found that a significant number of nuclei with homologs entirely paired in meiotic chromosome spreads from late 4th/early 5th instar larvae (Figure 2 and S5). This finding led us to wonder whether homolog pairing is more stable in *B. mori* female meiosis than previously appreciated. Like *Drosophila*, the *B. mori* larval ovary is composed of polytrophic meroistic ovarioles containing linear arrays of developing egg chambers, with the tip (germarium) harboring germ line stem cells that are mitotically dividing and the most mature chambers being the most distal from the stem cell niche ((62,72,73), Figure 6A and Figure S12). However, as moths have a much shorter adult lifespan than flies (only 5-7 days for silkmoths versus 2-3 months for *Drosophila*), the majority of oogenesis occurs in the larval and pupal stages (62).

To determine how long homologs remain paired end-to-end in meiotic prophase in females, we performed whole-mount DNA FISH with ch7 stripe paints in 5th instar larval ovaries. This approach yielded robust FISH signal throughout the developing egg chambers and in the germarium (Figure 6). In agreement with our initial observations from ovary squashes, we observed that all cells in the germarium harbor paired, linear homologs through early pachytene (Figure 6A-B). Interestingly, ch7 homologs were still paired end-to-end in late pachytene, where nurse cells and the developing

oocytes begin to differentiate (Figure 6C). The majority of oocytes in the developing egg chambers outside the germarium in 5th instar larvae are arrested in late diakinesis or metaphase I (57), which should be after transformation of the SC at the end of pachytene. Surprisingly, we observed that chromosome-wide pairing persists in all oocytes present in developing egg chambers throughout the length of the 5th instar larval ovarioles (Figure 6C-D). This finding suggests that, even in the absence of chiasma and with the partial breakdown and transformation of the SC, end-to-end pairing persists throughout meiotic prophase I in female *B. mori*. Altogether, these studies using Oligopaints in *B. mori* larval ovaries and testes demonstrate that this FISH-based approach is highly successful in both squashed and whole tissue and can be used to study chromosome dynamics throughout different stages of meiosis.

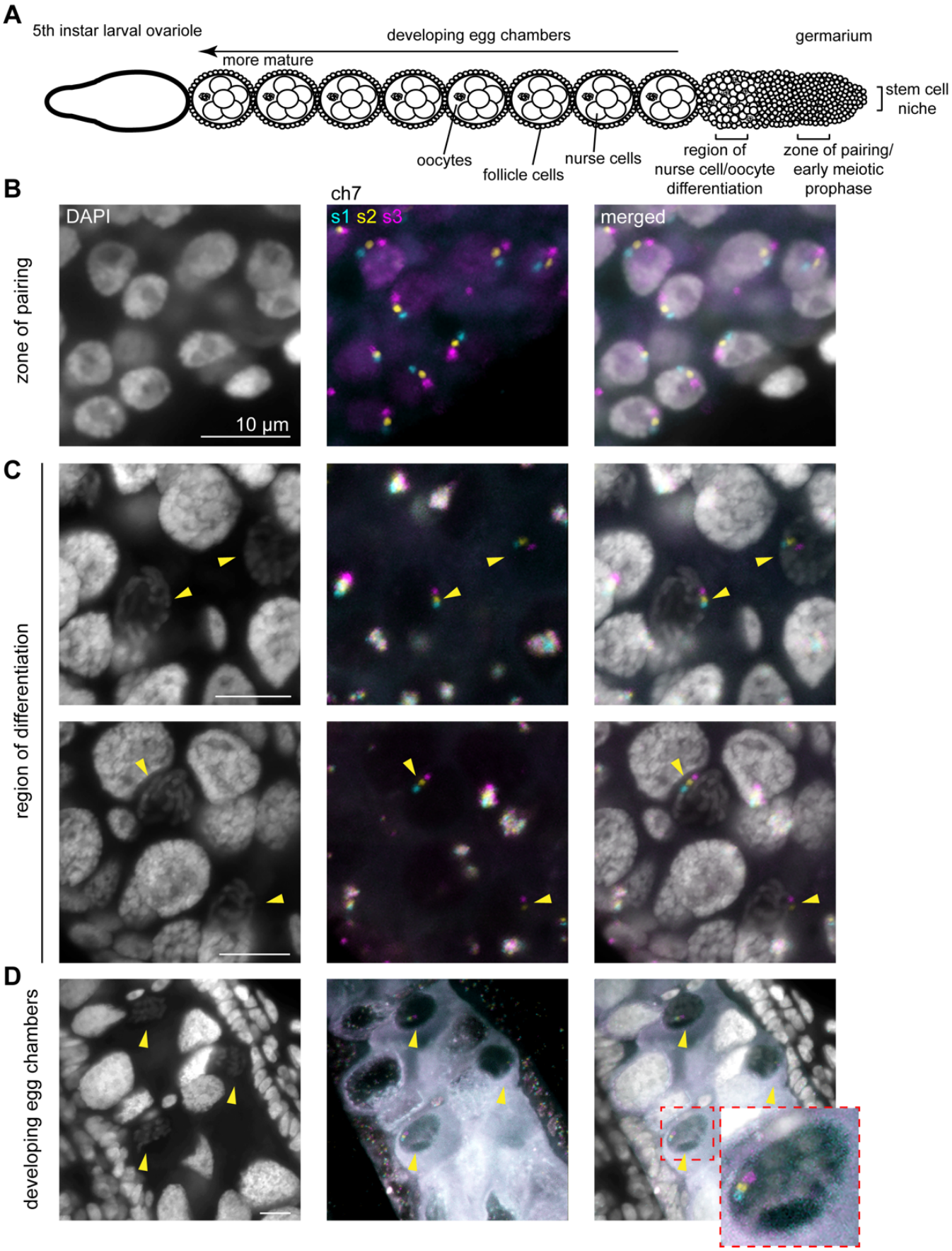

338

339

Figure 6. FISH with stripe chromosome paints in whole mount 5th instar larval ovary.
A) Schematic of ovariole from 5th instar *B. mori* larval ovary. B) Representative pachytene nuclei from germarium of larval ovary labeled with ch7 stripe paints. C) Representative fields showing early oocytes and early nurse cells labeled with ch7 stripe paints. Yellow arrowheads indicate oocytes. Chromosome wide pairing is still present in oocytes at this stage. D) Representative image showing mature (~stage 5) egg chambers. Yellow arrowheads indicate oocytes. Chromosome wide pairing is still present in oocytes at this late prophase stage.

Discussion

The silkworm, *B. mori*, has been a model system for studying meiotic chromosomes for decades. Like *Drosophila*, silkworms are readily reared in a laboratory setting and highly amenable to genetic manipulations including RNAi and CRISPR. However, unlike fruit flies, silkworms are large in size, combining the increased ease of dissection and structure visualization commonly associated with mammals with the short generation time of an insect system. Additionally, the large amount of tissue provided by *B. mori* increases the feasibility of genomics assays and other cell population-based approaches, which require a large number of cells. Importantly, the recent sequencing of the *B. mori* genome revealed that there is a high degree of sequence homology between silkworm genes and mammalian disease genes (61,74–76). Furthermore, *Bombyx* represents an excellent insect model system for studying meiosis, as SC constituents in non-Drosophilid arthropods are closely aligned with vertebrates, while *Drosophila* harbor a unique suite of SC factors (77,78). Finally, *B. mori* harbor 28 chromosomes while humans have 23 (and *Drosophila* have only 4), and our studies along with others have illustrated that homologs remain unpaired in *B. mori* somatic cells (79). This is in stark contrast to the high levels of somatic homolog pairing seen in *Drosophila* (80,81), making the study of *B. mori* genome dynamics more directly relevant to human biology.

Here, we take advantage of the *B. mori* model system to visualize single chromosome dynamics in meiosis using the Oligopaints technology. As previously described for *C. elegans*, we have utilized the flexibility and scalability of the Oligopaint design process to add chromosome-specific

barcodes to label either whole chromosomes or different sub-chromosomal loci using the same set of oligos (19). Using these multiplexed Oligopaints, we have provided the first extensive characterization of single, whole chromosomes in meiosis in both males and females in any species. Our studies show in great detail how chromosomes in larval testes condense, pair, and partially unpair to form metaphase I cruciform bivalents. While crossing over has been reported in male meiosis in *B. mori* (53,57), clear chiasmata were not apparent in post-pachytene spermatocytes using our imaging approach (Figure 2, 4, 5). We think this inability to detect chiasmata is likely due to the small size and compact nature of *B. mori* chromosomes in diplotene.

We show that mitotic chromosomes in *B. mori*, which are holocentric in structure, align parallel to the metaphase plate, with both telomeres being aligned with the plate and homologs being unpaired. Our studies further reveal that, like those in *C. elegans*, *B. mori* chromosomes do not retain the holocentric configuration in meiosis. Instead, meiotic chromosomes at metaphase I in spermatogenesis align perpendicular to the metaphase plate such that telomeric regions face the spindle poles and likely act as localized kinetochores. Moreover, we demonstrate that both telomeres are equally likely to face poleward and harbor kinetochore activity. A similar telokinetic approach to meiosis has also been observed in the holocentric milkweed bug *Oncopeltus fasciatus* (82) and the kissing bug *Triatoma infestans* (83). Whether crossover position dictates bivalent structure in *B. mori* or other holocentric insects, as in *C. elegans* (42,46,49–51), remains to be explored. Additionally, how the meiotic spindle attaches to *B. mori* chromosomes and what kinetochore proteins are involved is yet to be determined, although electron microscopy studies have suggested that microtubules directly penetrate the poleward surface of chromosomes during spermatogenesis (52). Interestingly, the broadly conserved centromere-specific histone H3 variant CENP-A is absent from the genome of Lepidopteran insects (56), suggesting that both mitotic and meiotic chromosome segregation in *Bombyx* are independent of CENP-A.

We determine that chromosome-wide pairing in *B. mori* female meiosis is more stable than previously appreciated and persists throughout the entirety of meiotic prophase. How chromosomes remain paired end-to-end, even after loss of the central elements of the SC and through SC transformation, remains unclear. Finally, in addition to demonstrating the feasibility of using Oligopaints to study meiotic chromosomes, our studies illustrate that Oligopaints can be designed for species with draft genome assemblies and that the Oligopaints can in turn be used to validate both inter- and intra-chromosome level genome assemblies.

Materials and Methods

B. mori strains and cell line

Embryos were obtained from Carolina Biological (Burlington, NC), Coastal Silkworms (Jacksonville, FL), Mulberry Farms (Fallbrook, CA), or were freshly laid in the lab from larvae derived from embryos from these sources. Some larvae were obtained from Rainbow Mealworms (Compton, CA). Embryos were kept at 4˚C for less than 1 month. For rearing, embryos were transferred to 28˚C and larvae were fed fresh mulberry leaves or powdered mulberry chow (Carolina Biological or Rainbow Mealworms). BmN4 cells are commercially available from ATCC (Manassas, VA).

Oligopaint design and synthesis

Oligopaint libraries were designed as described in the main text. Active and inactive domains were determined primarily based on CENP-T depletion or enrichment. CENP-T ChIP-seq profiles were obtained from BmN4 cells and domains were called as previously described (37) with the following modifications: CENP-T ChIP-seq signal originally in 10 kb windows was averaged over 50 kb. Subsequently, negative CENP-T domains were subtracted from positive CENP-T domains to obtain

final CENP-T depleted domains. As previously observed, domains enriched for CENP-T were shown to strongly correlate with enrichment for the repressive histone mark H3K27me3, while domains depleted of CENP-T were shown to strongly correlate with enrichment of the active chromatin marks H3K4me3 and H3K36me3. All information regarding genomic coordinates for Oligopaints and probe density can be found in Tables 1-5. Oligo pools were purchased from CustomArray/GenScript (Redmond, WA; ch 7, 15, 16) or Twist Biosciences (San Francisco, CA; ch 4, 17, 23, Z). Oligopaints were synthesized as previously described by adding barcodes to each oligo for PCR-based amplification (17,30,84).

Table 1. Chromosome and chromosome paint information

Chrom.	chromosome size (bp)	size painted (bp)	paint start	paint stop	density (probes/kb)	total # of oligos
4	18737234	18639239	282	18639521	1.5	26841
7	13944894	13868845	35931	13904776	3	42625
15	18440292	18354755	21089	18375844	1	17756
16	14337292	14275583	27737	14303320	1.5	20190
17	16840672	16806551	9415	16815966	1.5	23834
23	21465692	21339065	123188	21462253	1.5	30506
Z (1)	20666287	20578020	37936	20615956	1.5	29784

Table 2. Stripe sub-library paint information

Chrom. and stripe	paint start	paint stop	Stripe size (Mb)
7 stripe 1	35931	2809682	2.77
7 stripe 2	5587874	8357288	2.76
7 stripe 3	11131025	13904776	2.77
15 stripe 1	21089	3684775	3.66
15 stripe 2	7380341	11061106	3.68
15 stripe 3	14748412	18375844	3.62
23 stripe 1	123188	1638259	1.51
23 stripe 2	9909172	11556867	1.65
23 stripe 3	19815237	21462253	1.65
Z stripe 1	37936	1589202	1.55
Z stripe 2	9538407	11119201	1.58
Z stripe 3	19078122	20615956	1.53

429 **Table 3. Ch7 Active and inactive chromatin domains paint information**
430

Domain	Start	Stop	Size (bp)
inactive	35931	800000	764070
active	800001	900000	100000
inactive	1000001	1100000	100000
active	1100001	1250000	150000
inactive	1300001	1500000	200000
active	1500001	1600000	100000
inactive	1600001	1700000	100000
active	1700001	1850000	150000
inactive	1850001	1900000	50000
active	1950001	2000000	50000
inactive	2000001	2300000	300000
inactive	2400001	2600000	200000
active	2600001	2700000	100000
inactive	2700001	3350000	650000
active	3400001	3650000	250000
inactive	3650001	3900000	250000
active	3900001	4000000	100000
inactive	4000001	4550000	550000
active	4550001	4650000	100000
inactive	4650001	4950000	300000
active	4950001	5400000	450000
inactive	5450001	5800000	350000
active	5900001	6050000	150000
inactive	6050001	6250000	200000
inactive	6300001	6450000	150000
active	6450001	6550000	100000
inactive	6550001	6650000	100000
active	6700001	6800000	100000
active	6850001	7150000	300000
inactive	7150001	7400000	250000
active	7400001	7600000	200000
inactive	7600001	7900000	300000
active	7950001	8200000	250000
inactive	8250001	8750000	500000
inactive	8800001	9050000	250000
active	9050001	9300000	250000
inactive	9350001	9400000	50000
active	9400001	9550000	150000
inactive	9650001	10800000	1150000
active	10850001	11100000	250000
active	11150001	11400000	250000
inactive	11400001	11650000	250000
active	11650001	11950000	300000
inactive	11950001	12300000	350000
active	12300001	12600000	300000
inactive	12600001	12700000	100000
active	12700001	12750000	50000
inactive	12800001	12950000	150000
active	12950001	13150000	200000
inactive	13150001	13250000	100000
active	13350001	13450000	100000

inactive	13500001	13650000	150000
active	13700001	13849955	149955

431
432
433 **Table 4. Ch15 Active and inactive chromatin domains paint information**
434

Domain	Start	Stop	Size (bp)
inactive	21089	200000	178912
active	250001	850000	600000
active	900001	1000000	100000
inactive	1000001	1400000	400000
active	1400001	1950000	550000
inactive	1950001	2250000	300000
active	2250001	2550000	300000
inactive	2550001	2800000	250000
active	2850001	3200000	350000
inactive	3200001	3500000	300000
active	3550001	3850000	300000
inactive	3850001	3900000	50000
active	3950001	4100000	150000
inactive	4100001	4250000	150000
active	4250001	4350000	100000
inactive	4350001	4650000	300000
active	4650001	4750000	100000
inactive	4750001	4950000	200000
inactive	5000001	5150000	150000
active	5150001	5250000	100000
inactive	5300001	5350000	50000
active	5350001	6100000	750000
inactive	6100001	6200000	100000
active	6250001	6500000	250000
inactive	6500001	6700000	200000
active	6700001	6850000	150000
inactive	6900001	7100000	200000
active	7100001	7300000	200000
inactive	7300001	7550000	250000
active	7550001	7800000	250000
inactive	7800001	8100000	300000
active	8100001	8300000	200000
inactive	8400001	8650000	250000
active	8650001	8750000	100000
inactive	8750001	8800000	50000
active	8850001	8900000	50000
inactive	8900001	9100000	200000
active	9100001	9500000	400000
inactive	9500001	9550000	50000
active	9600001	9750000	150000
active	9800001	9950000	150000
inactive	10000001	10500000	500000
active	10500001	11200000	700000
active	11350001	11400000	50000
inactive	11400001	11500000	100000
active	11500001	11950000	450000

inactive	11950001	12000000	50000
active	12050001	12200000	150000
inactive	12200001	12250000	50000
active	12300001	12500000	200000
inactive	12500001	12600000	100000
active	12600001	12850000	250000
inactive	12850001	12950000	100000
active	12950001	13400000	450000
inactive	13450001	13600000	150000
active	13650001	13750000	100000
inactive	13750001	14150000	400000
inactive	14200001	14850000	650000
active	14900001	15050000	150000
inactive	15100001	15250000	150000
active	15300001	15500000	200000
inactive	15550001	15600000	50000
active	15600001	15750000	150000
inactive	15750001	16000000	250000
inactive	16050001	16350000	300000
inactive	16400001	17850000	1450000
inactive	17900001	18100000	200000
active	18150001	18200000	50000
inactive	18200001	18250000	50000
active	18300001	18350000	50000
inactive	18350001	18375844	25844

435
436
437 **Table 5. Ch16 Active and inactive chromatin domains paint information**
438

Domain	Start	Stop	Size (bp)
inactive	27737	50000	22264
active	50001	150000	100000
inactive	150001	250000	100000
active	250001	350000	100000
inactive	350001	650000	300000
active	700001	1350000	650000
inactive	1400001	1700000	300000
active	1700001	2300000	600000
inactive	2300001	2400000	100000
active	2400001	2700000	300000
inactive	2700001	3200000	500000
active	3200001	3600000	400000
inactive	3600001	4050000	450000
active	4050001	4200000	150000
inactive	4200001	4500000	300000
active	4500001	4600000	100000
active	4700001	4750000	50000
inactive	4750001	4800000	50000
active	4900001	4950000	50000
active	5000001	5250000	250000
inactive	5250001	5600000	350000
active	5600001	6000000	400000
inactive	6000001	6150000	150000
active	6200001	6250000	50000

active	6300001	6500000	200000
active	6550001	6650000	100000
inactive	6650001	6850000	200000
active	6850001	7000000	150000
inactive	7050001	7950000	900000
inactive	8000001	8500000	500000
active	8550001	8750000	200000
inactive	8800001	8900000	100000
active	8900001	9400000	500000
inactive	9400001	9450000	50000
active	9500001	10100000	600000
inactive	10100001	11450000	1350000
active	11450001	11550000	100000
inactive	11550001	11900000	350000
active	11950001	12250000	300000
inactive	12250001	12400000	150000
active	12400001	12500000	100000
inactive	12500001	12700000	200000
active	12750001	13200000	450000
inactive	13250001	13800000	550000
active	13800001	14100000	300000
inactive	14100001	14303320	203320

Preparation of meiotic chromosome spreads and DNA FISH

For meiotic squashes, late 4th instar or early 5th instar larvae (approximately 3 inches in length) were sacrificed by decapitation. The caterpillars where then cut open anterior to posterior and fileted on a silicone dissecting dish using standard sewing needles. Gonads were harvested using forceps and placed into 1.5 mL tubes containing SF900 tissue culture media. Gonads were then rinsed thrice in 1X PBS, then incubated in 1X PBS+0.5% sodium citrate for 8-10 min. Using forceps, gonads were then transferred to siliconized coverslips (1 gonad per coverslip) and covered with ~10 μL of 45% acetic acid/1% PFA/1X PBS and fixed for 6 min. Using a poly-L-lysine coated glass slide, gonads were then physically squashed and slide/coverslip were flash frozen in liquid nitrogen. After carefully removing slides from liquid nitrogen, coverslips were removed with a razor blade, and slides were post-fixed in cold (pre-chilled to -20°C) 3:1 methanol:glacial acetic acid for 10 min. After fixation, slides were washed thrice in 1X PBS and subjected to an ethanol row at -20°C (70%, 90%, 100% ethanol, 5 min each) before drying completely at room temp. Slides were dried for 24-72 h.

454 FISH on meiotic squashes was performed as previously described for mitotic spreads (31).
455 Briefly, after drying slides, slides were denatured at 72°C for 2.5 min in 2xSSCT/70% formamide
456 before again drying with an ethanol row at -20°C. Slides were then left to air dry for 10 min at room
457 temperature. Primary Oligopaint probes were resuspended in hybridization buffer (10% dextran
458 sulfate/2xSSCT/50% formamide/4% polyvinylsulfonic acid), placed on slides, covered with a coverslip,
459 and sealed with rubber cement. Slides were denatured on a heat block in a water bath set to 92°C for
460 2.5 min, after which slides were transferred to a humidified chamber and incubated at 37°C
461 overnight. The next day, coverslips were removed using a razor blade and slides were washed as
462 follows: 2×SSCT at 60°C for 15 min, 2×SSCT at RT for 15 min, and 0.2×SSC at RT for 5 min.
463 Fluorescently labeled secondary probes were then added to slides, again resuspended in
464 hybridization buffer, covered with a coverslip, and sealed with rubber cement. Slides were incubated
465 at 37°C for 2 h in a humidified chamber, before repeating the above washes. All slides were stained
466 DAPI and mounted in Prolong Diamond (Invitrogen/ThermoFisher, Waltham, MA). Slides were cured
467 overnight before sealing with clear nail polish and imaging.
468
469 **FISH on whole-mount gonads and embryos**
470 For whole-mount DNA FISH in gonads, ovaries and testes from late 5th instar larvae (after
471 secession of eating) were dissected in SF900 cell culture media, washed thrice briefly with 1X PBS,
472 and then fixed for 30 min in 4% PFA in PBS with 0.1% Triton-X-100 (0.1% PBS-T) at RT. Gonads were
473 then washed again thrice in 1X PBS and permeabilized with 0.5% PBS-T for 15 min at RT. Gonads were
474 pre-denatured by washing as follows: 2xSSCT for 10 min at RT, 2xSSCT/20% formamide for 10 min at
475 RT, 2xSSCT/50% formamide for 10 min at RT, 2xSSCT/50% formamide for 3 h at 37°C, 2xSSCT/50%
476 formamide for 3 min at 92°C, 2xSSCT/50% formamide for 20 min at 60°C. To the 2xSSCT/50%
477 formamide, 100 pmol of each probe was directly added. Gonads were then denatured at for 3 min at

92°C and incubated overnight at 37°C. The next day, gonads were washed: 3x 30 min each in 2xSSCT/50% formamide at 37°C, 1x 15 min in 2xSSCT at RT. 20 pmol of each secondary oligo was added with 50% formamide and incubated for 3 h at 37°C. Final washes were performed (2x 30 min in 2xSSCT/50% formamide at 37°C, 1x 10 min in 2xSSCT/50% formamide at RT, 1x 10 min in 2xSSCT/20% formamide at RT, 1x 10 min in 2xSSCT at RT), gonads were stained with DAPI, and mounted on slides with Prolong Diamond (Invitrogen/ThermoFisher).

For whole-mount embryo FISH, diapausing embryos were removed from 4°C and kept at RT for 3-5 d. Chorions were weakened by soaking in 50% bleach for 15 min and then manually removed with forceps. Embryos were subsequently fixed for 30 min in 4% PFA in 0.1% PBS-T at RT, and FISH was performed as described above for whole-mount gonads.

Meiotic staging

Stages of meiosis were determined based largely on DAPI morphology and/or cell position in whole-mount gonads. Late 4th-early 5th instar male larvae were used for squashes as they only possess primary spermatocytes in meiosis I. In whole-mount testes, meiosis I and II were distinguished based on position in the gonad and based on the number of cells per bundle (with meiosis I bundles harboring approximately 64 cells and meiosis II bundles harboring approximately 128 cells).

Mitotic spreads from BmN4 cells

To induce mitotic arrest, approximately 1 × 10^5 cells were treated with 0.5 µg/mL Colcemid Solution (Gibco/ThermoFisher) for 2 h in a 28˚C heat block. Cells were then spun for 5 min at 600 x *g* at room temperature to pellet and resuspended in hypotonic solution (500 mL of 0.5% sodium citrate). Cells were incubated in hypotonic solution for 8 min. 100 µL of the cell suspension were then

placed in a cytofunnel and spun at 1200 rpm for 5 min with high acceleration using a cytocentrifuge (Shandon Cytospin 4; ThermoFisher). For FISH, slides were then fixed in cold 3:1 methanol: acetic acid for 10 min and washed 3 times for 5 min in PBS-T (PBS with 0.1% Triton X-100). FISH was performed as described above for meiotic spreads.

Imaging, quantification, and data analysis

Images of meiotic squashes were acquired on a Leica DMi6000 wide-field inverted fluorescence microscope using an HCX PL APO 63x/1.40-0.60 Oil objective (Leica Biosystems, Buffalo Grove, IL), Leica DFC9000 sCMOS Monochrome Camera, and LasX software. Whole mount images were acquired using a Zeiss LSM 780 point scanning confocal (Zeiss Microscope Systems, Jena, Germany) with high sensitivity 32 anode Hybrid-GaAsP detectors. BmN4 mitotic spreads were acquired on a Zeiss AxioObserver Z1 wide-field inverted fluorescence microscope with 100x/1.4 oil Plan-APO objective, a Hamamatsu C13440 ORCA-Flash 4.0 V3 Digital CMOS camera, and ZEN blue software. Images were processed using Huygens deconvolution software (SVI, Hilversum, Netherlands), and tiffs were created in ImageJ. Meiotic bivalent quantification was performed manually.

Acknowledgements

We would like to thank the members of the Lei and Drinnenberg labs, as well as Jamie Walters, Petr Nguyen, and Martina Dalikova for helpful discussion. We would also like to thank Stacie Hughes, Scott Hawley, Jean-René Huynh, and Anahi Molla-Herman for critical reading of the manuscript.

Funding

This work was funded by the Intramural Program of the National Institute of Diabetes and Digestive and Kidney Diseases, National Institutes of Health (DK015602 to E.P.L.), and by LabEx DEEP (ANR-11-LABX-0044, ANR-10-IDEX-0001-02 to I.A.D.), an ATIP-AVENIR research grant, Institut Curie, the CNRS and the ERC (CENEVO-758757 to I.A.D.). The funders had no role in study design, data collection and analysis, decision to publish, or preparation of the manuscript.

Competing Interests

The authors declare no competing interests.

References

1. Bascom-Slack CA, Ross LO, Dawson DS. Chiasmata, crossovers, and meiotic chromosome segregation. Adv Genet. 1997;35:253–84.

2. Fawcett DW. THE FINE STRUCTURE OF CHROMOSOMES IN THE MEIOTIC PROPHASE OF VERTEBRATE SPERMATOCYTES. The Journal of Biophysical and Biochemical Cytology. 1956 Jul 25;2(4):403–6.

3. Moses MJ. Chromosomal Structures in Crayfish Spermatocytes. J Biophys Biochem Cytol. 1956 Mar 25;2(2):215–8.

4. Agostinho A, Kouznetsova A, Hernández-Hernández A, Bernhem K, Blom H, Brismar H, et al. Sexual dimorphism in the width of the mouse synaptonemal complex. J Cell Sci. 2018 Mar 1;131(5):jcs212548.

5. Cahoon CK, Yu Z, Wang Y, Guo F, Unruh JR, Slaughter BD, et al. Superresolution expansion microscopy reveals the three-dimensional organization of the Drosophila synaptonemal complex. Proc Natl Acad Sci USA. 2017 15;114(33):E6857–66.

6. Capilla-Pérez L, Durand S, Hurel A, Lian Q, Chambon A, Taochy C, et al. The synaptonemal complex imposes crossover interference and heterochiasmy in Arabidopsis. PNAS [Internet]. 2021 Mar 23 [cited 2021 Mar 17];118(12). Available from: https://www.pnas.org/content/118/12/e2023613118

7. Qiao H, Chen JK, Reynolds A, Höög C, Paddy M, Hunter N. Interplay between Synaptonemal Complex, Homologous Recombination, and Centromeres during Mammalian Meiosis. PLOS Genetics. 2012 Jun 28;8(6):e1002790.

8. Xu H, Tong Z, Ye Q, Sun T, Hong Z, Zhang L, et al. Molecular organization of mammalian meiotic chromosome axis revealed by expansion STORM microscopy. PNAS. 2019 Sep 10;116(37):18423–8.

9. Yoon S, Choi E-H, Kim J-W, Kim KP. Structured illumination microscopy imaging reveals localization of replication protein A between chromosome lateral elements during mammalian meiosis. Exp Mol Med. 2018 Aug 28;50(8):1–12.

10. Blokhina YP, Nguyen AD, Draper BW, Burgess SM. The telomere bouquet is a hub where meiotic double-strand breaks, synapsis, and stable homolog juxtaposition are coordinated in the zebrafish, Danio rerio. PLOS Genetics. 2019 Jan 17;15(1):e1007730.

11. Bisig CG, Guiraldelli MF, Kouznetsova A, Scherthan H, Höög C, Dawson DS, et al. Synaptonemal Complex Components Persist at Centromeres and Are Required for Homologous Centromere Pairing in Mouse Spermatocytes. PLOS Genetics. 2012 Jun 28;8(6):e1002701.

12. Christophorou N, Rubin T, Huynh J-R. Synaptonemal complex components promote centromere pairing in pre-meiotic germ cells. PLoS Genet. 2013;9(12):e1004012.

13. Boateng KA, Bellani MA, Gregoretti IV, Pratto F, Camerini-Otero RD. Homologous Pairing Preceding SPO11 Mediated Double Strand Breaks in Mice. Dev Cell. 2013 Jan 28;24(2):196–205.

14. Ishiguro K, Kim J, Shibuya H, Hernández-Hernández A, Suzuki A, Fukagawa T, et al. Meiosis-specific cohesin mediates homolog recognition in mouse spermatocytes. Genes Dev. 2014 Mar 15;28(6):594–607.

15. Scherthan J, Bahler J, Kohli. Dynamics of chromosome organization and pairing during meiotic prophase in fission yeast. J Cell Biol. 1994 Oct 2;127(2):273–85.

16. Joyce EF, Apostolopoulos N, Beliveau BJ, Wu C -ting. Germline Progenitors Escape the Widespread Phenomenon of Homolog Pairing during Drosophila Development. PLoS Genet. 2013 Dec 19;9(12):e1004013.

17. Nguyen SC, Joyce EF. Programmable Chromosome Painting with Oligopaints. In: Shav-Tal Y, editor. Imaging Gene Expression: Methods and Protocols [Internet]. New York, NY: Springer New York; 2019 [cited 2019 Aug 14]. p. 167–80. (Methods in Molecular Biology). Available from: https://doi.org/10.1007/978-1-4939-9674-2_11

18. Beliveau BJ, Joyce EF, Apostolopoulos N, Yilmaz F, Fonseka CY, McCole RB, et al. Versatile design and synthesis platform for visualizing genomes with Oligopaint FISH probes. Proc Natl Acad Sci USA. 2012 Dec 26;109(52):21301–6.

19. Fields BD, Nguyen SC, Nir G, Kennedy S. A multiplexed DNA FISH strategy for assessing genome architecture in Caenorhabditis elegans. eLife [Internet]. 2019 May 14 [cited 2019 Jun 5];8. Available from: https://elifesciences.org/articles/42823

20. Albert PS, Zhang T, Semrau K, Rouillard J-M, Kao Y-H, Wang C-JR, et al. Whole-chromosome paints in maize reveal rearrangements, nuclear domains, and chromosomal relationships. Proc Natl Acad Sci U S A. 2019 Jan 29;116(5):1679–85.

21. Beliveau BJ, Boettiger AN, Avendaño MS, Jungmann R, McCole RB, Joyce EF, et al. Single-molecule super-resolution imaging of chromosomes and in situ haplotype visualization using Oligopaint FISH probes. Nature Communications. 2015 May 12;6(1):7147.

22. Beliveau BJ, Boettiger AN, Nir G, Bintu B, Yin P, Zhuang X, et al. In Situ Super-Resolution Imaging of Genomic DNA with OligoSTORM and OligoDNA-PAINT. Methods Mol Biol. 2017;1663:231–52.

23. Bintu B, Mateo LJ, Su J-H, Sinnott-Armstrong NA, Parker M, Kinrot S, et al. Super-resolution chromatin tracing reveals domains and cooperative interactions in single cells. Science. 2018 Oct 26;362(6413).

24. Boettiger AN, Bintu B, Moffitt JR, Wang S, Beliveau BJ, Fudenberg G, et al. Super-resolution imaging reveals distinct chromatin folding for different epigenetic states. Nature. 2016 Jan;529(7586):418–22.

25. Boyle S, Rodesch MJ, Halvensleben HA, Jeddeloh JA, Bickmore WA. Fluorescence in situ hybridization with high-complexity repeat-free oligonucleotide probes generated by massively parallel synthesis. Chromosome Res. 2011 Oct 18;19(7):901–9.

26. Han Y, Zhang T, Thammapichai P, Weng Y, Jiang J. Chromosome-Specific Painting in Cucumis Species Using Bulked Oligonucleotides. Genetics. 2015 Jul;200(3):771–9.

27. Joyce EF, Williams BR, Xie T, Wu C -ting. Identification of Genes That Promote or Antagonize Somatic Homolog Pairing Using a High-Throughput FISH–Based Screen. PLOS Genetics. 2012 May 10;8(5):e1002667.

28. Luppino JM, Park DS, Nguyen SC, Lan Y, Xu Z, Yunker R, et al. Cohesin promotes stochastic domain intermingling to ensure proper regulation of boundary-proximal genes. Nature Genetics. 2020 Aug;52(8):840–8.

29. Qu M, Li K, Han Y, Chen L, Li Z, Han Y. Integrated Karyotyping of Woodland Strawberry (Fragaria vesca) with Oligopaint FISH Probes. Cytogenet Genome Res. 2017;153(3):158–64.

30. Rosin LF, Nguyen SC, Joyce EF. Condensin II drives large-scale folding and spatial partitioning of interphase chromosomes in Drosophila nuclei. PLoS Genet. 2018;14(7):e1007393.

31. Rosin LF, Crocker O, Isenhart RL, Nguyen SC, Xu Z, Joyce EF. Chromosome territory formation attenuates the translocation potential of cells. Dernburg AF, Struhl K, Bosco G, editors. eLife. 2019 Nov 4;8:e49553.

32. Hylton CA, Hansen K, Bourgeois A, Dean JET. Sex Chromosome Pairing Mediated by Euchromatic Homology in Drosophila Male Meiosis. Genetics. 2020 Mar 1;214(3):605–16.

33. do Vale Martins L, Yu F, Zhao H, Dennison T, Lauter N, Wang H, et al. Meiotic crossovers characterized by haplotype-specific chromosome painting in maize. Nature Communications. 2019 Oct 10;10(1):4604.

34. Cortes-Silva N, Ulmer J, Kiuchi T, Hsieh E, Cornilleau G, Ladid I, et al. CenH3-Independent Kinetochore Assembly in Lepidoptera Requires CCAN, Including CENP-T. Current Biology. 2020 Feb 24;30(4):561-572.e10.

35. Mon H, Lee JM, Mita K, Goldsmith MR, Kusakabe T. Chromatin-induced spindle assembly plays an important role in metaphase congression of silkworm holocentric chromosomes. Insect Biochem Mol Biol. 2014 Feb;45:40–50.

36. Murakami A, Imai HT. Cytological evidence for holocentric chromosomes of the silkworms, Bombyx mori and B. mandarina, (Bombycidae, Lepidoptera). Chromosoma. 1974;47(2):167–78.

37. Senaratne AP, Muller H, Fryer KA, Kawamoto M, Katsuma S, Drinnenberg IA. Formation of the CenH3-Deficient Holocentromere in Lepidoptera Avoids Active Chromatin. Current Biology [Internet]. 2020 Oct 29 [cited 2020 Dec 9]; Available from: http://www.sciencedirect.com/science/article/pii/S0960982220314482

38. Moore LL, Morrison M, Roth MB. HCP-1, a protein involved in chromosome segregation, is localized to the centromere of mitotic chromosomes in Caenorhabditis elegans. J Cell Biol. 1999 Nov 1;147(3):471–80.

39. Albertson DG, Thomson JN. The kinetochores of Caenorhabditis elegans. Chromosoma. 1982;86(3):409–28.

40. Melters DP, Paliulis LV, Korf IF, Chan SWL. Holocentric chromosomes: convergent evolution, meiotic adaptations, and genomic analysis. Chromosome Res. 2012 Jul 1;20(5):579–93.

41. Heckmann S, Jankowska M, Schubert V, Kumke K, Ma W, Houben A. Alternative meiotic chromatid segregation in the holocentric plant Luzula elegans. Nat Commun. 2014 Oct 8;5:4979.

42. Albertson DG, Thomson JN. Segregation of holocentric chromosomes at meiosis in the nematode, Caenorhabditis elegans. Chromosome Res. 1993 May;1(1):15–26.

43. Dumont J, Oegema K, Desai A. A kinetochore-independent mechanism drives anaphase chromosome separation during acentrosomal meiosis. Nat Cell Biol. 2010 Sep;12(9):894–901.

44. Maddox PS, Oegema K, Desai A, Cheeseman IM. “Holo”er than thou: chromosome segregation and kinetochore function in C. elegans. Chromosome Res. 2004;12(6):641–53.

45. Melters DP, Paliulis LV, Korf IF, Chan SWL. Holocentric chromosomes: convergent evolution, meiotic adaptations, and genomic analysis. Chromosome Res. 2012 Jul 1;20(5):579–93.

46. Schvarzstein M, Wignall SM, Villeneuve AM. Coordinating cohesion, co-orientation, and congression during meiosis: lessons from holocentric chromosomes. Genes Dev. 2010 Feb 1;24(3):219–28.

659 47. Shakes DC, Wu J, Sadler PL, LaPrade K, Moore LL, Noritake A, et al. Spermatogenesis-Specific
660 Features of the Meiotic Program in Caenorhabditis elegans. PLOS Genetics. 2009 Aug
661 21;5(8):e1000611.

662 48. Wignall SM, Villeneuve AM. Lateral microtubule bundles promote chromosome alignment
663 during acentrosomal oocyte meiosis. Nat Cell Biol. 2009 Jul;11(7):839–44.

664 49. Albertson DG, Rose AM, Villeneuve AM. Chromosome Organization, Mitosis, and Meiosis. In:
665 Riddle DL, Blumenthal T, Meyer BJ, Priess JR, editors. C elegans II [Internet]. 2nd ed. Cold Spring
666 Harbor (NY): Cold Spring Harbor Laboratory Press; 1997 [cited 2021 Jan 13]. Available from:
667 http://www.ncbi.nlm.nih.gov/books/NBK20058/

668 50. Martinez-Perez E, Schvarzstein M, Barroso C, Lightfoot J, Dernburg AF, Villeneuve AM.
669 Crossovers trigger a remodeling of meiotic chromosome axis composition that is linked to two-
670 step loss of sister chromatid cohesion. Genes Dev. 2008 Oct 15;22(20):2886–901.

671 51. Monen J, Maddox PS, Hyndman F, Oegema K, Desai A. Differential role of CENP-A in the
672 segregation of holocentric C. elegans chromosomes during meiosis and mitosis. Nat Cell Biol.
673 2005 Dec;7(12):1248–55.

674 52. Friedländer M, Wahrman J. The spindle as a basal body distributor. A study in the meiosis of the
675 male silkworm moth, Bombyx mori. J Cell Sci. 1970 Jul;7(1):65–89.

676 53. Holm PB, Rasmussen SW. Chromosome pairing, recombination nodules and chiasma formation
677 in diploid Bombyx males. Carlsberg Res Commun. 1980 Nov 1;45(6):483.

678 54. Rasmussen SW, Holm PB. The Meiotic Prophase in Bombyx mori. In: King RC, Akai H, editors.
679 Insect Ultrastructure: Volume 1 [Internet]. Boston, MA: Springer US; 1982 [cited 2021 Jan 12]. p.
680 61–85. Available from: https://doi.org/10.1007/978-1-4615-7266-4_3

681 55. Fielder SM, Kempfer R, Kelly WG. Multiple Sex-Specific Differences in the Regulation of Meiotic
682 Progression in C. elegans. bioRxiv. 2020 Mar 14;2020.03.12.989418.

683 56. Drinnenberg IA, deYoung D, Henikoff S, Malik HS. Recurrent loss of CenH3 is associated with
684 independent transitions to holocentricity in insects. Elife. 2014;3.

685 57. Maeda T. Chiasma Studies in the Silkworm, *Bombyx mori* L. The Japanese journal of genetics.
686 1939;15(3):118–27.

687 58. Rasmussen SW. The meiotic prophase in Bombyx mori females analyzed by three-dimensional
688 reconstructions of synaptonemal complexes. Chromosoma. 1976 Sep 1;54(3):245–93.

689 59. Rasmussen SW. The transformation of the synaptonemal complex into the “elimination
690 chromatin” in Bombyx mori oocytes. Chromosoma. 1977 Sep 1;60(3):205–21.

691 60. Beliveau BJ, Kishi JY, Nir G, Sasaki HM, Saka SK, Nguyen SC, et al. OligoMiner provides a rapid,
692 flexible environment for the design of genome-scale oligonucleotide in situ hybridization probes.
693 Proc Natl Acad Sci USA. 2018 06;115(10):E2183–92.

694 61. Kawamoto M, Jouraku A, Toyoda A, Yokoi K, Minakuchi Y, Katsuma S, et al. High-quality genome
695 assembly of the silkworm, Bombyx mori. Insect Biochemistry and Molecular Biology. 2019 Apr
696 1;107:53–62.

697 62. Beckemeyer EF, Shirk PD. Development of the larval ovary in the moth, Plodia interpunctella.
698 Journal of Insect Physiology. 2004 Nov 1;50(11):1045–51.

699 63. Page SL, Hawley RS. Chromosome Choreography: The Meiotic Ballet. Science. 2003 Aug
700 8;301(5634):785–9.

701 64. Pawlowski WP, Cande WZ. Coordinating the events of the meiotic prophase. Trends in Cell
702 Biology. 2005 Dec 1;15(12):674–81.

703 65. Chen S, Liu Y, Yang X, Liu Z, Luo X, Xu J, et al. Dysfunction of dimorphic sperm impairs male
704 fertility in the silkworm. Cell Discovery. 2020 Sep 8;6(1):1–15.

705 66. Friedlander M, Seth RK, Reynolds SE. Eupyrene and apyrene sperm: Dichotomous
706 spermatogenesis in Lepidoptera. Advances in Insect Physiology, Vol 32. 2005;206–308.

707 67. Friedländer M. Control of the eupyrene-apyrene sperm dimorphism in Lepidoptera. J Insect
708 Physiol. 1997 Nov;43(12):1085–92.

709 68. Meves F. Ueber oligopyrene und apyrene spermien und über ihre Entstehung, nach
710 Beobachtungen an Paludina und Pygaera. Arch f Mikrosk Anat. 1902;61:1–84.

711 69. Sahara K, Kawamura N. Double copulation of a female with sterile diploid and polyploid males
712 recovers fertility in Bombyx mori. Zygote. 2002 Feb;10(1):23–9.

713 70. Sahara K, Kawamura N. Roles of actin networks in peristaltic squeezing of sperm bundles in
714 Bombyx mori. J Morphol. 2004 Jan;259(1):1–6.

715 71. Sakai H, Oshima H, Yuri K, Gotoh H, Daimon T, Yaginuma T, et al. Dimorphic sperm formation by
716 Sex-lethal. PNAS. 2019 May 21;116(21):10412–7.

717 72. King RC, Aggarwal SK, Aggarwal U. The development of the female Drosophila reproductive
718 system. Journal of Morphology. 1968;124(2):143–65.

719 73. Paul S, Keshan B. Ovarian Development and Vitellogenin Gene Expression under Heat Stress in
720 Silkworm, Bombyx mori [Internet]. Vol. 2016, Psyche. Hindawi; 2016 [cited 2021 Feb 26]. p.
721 e4242317. Available from: https://www.hindawi.com/journals/psyche/2016/4242317/

722 74. Meng X, Zhu F, Chen K. Silkworm: A Promising Model Organism in Life Science. J Insect Sci
723 [Internet]. 2017 Oct 9 [cited 2020 Apr 25];17(5). Available from:
724 https://www.ncbi.nlm.nih.gov/pmc/articles/PMC5633739/

725 75. Mita K, Kasahara M, Sasaki S, Nagayasu Y, Yamada T, Kanamori H, et al. The genome sequence of
726 silkworm, Bombyx mori. DNA Res. 2004 Feb 29;11(1):27–35.

76. Xia Q, Zhou Z, Lu C, Cheng D, Dai F, Li B, et al. A draft sequence for the genome of the domesticated silkworm (Bombyx mori). Science. 2004 Dec 10;306(5703):1937–40.

77. Hemmer LW, Blumenstiel JP. Holding it together: rapid evolution and positive selection in the synaptonemal complex of Drosophila. BMC Evolutionary Biology. 2016 May 5;16(1):91.

78. Tromer EC, Wemyss TA, Waller RF, Akiyoshi B. Repurposing of Synaptonemal Complex Proteins for Kinetochores in Kinetoplastida. bioRxiv. 2021 Feb 6;2021.02.06.430040.

79. King TD, Leonard CJ, Cooper JC, Nguyen S, Joyce EF, Phadnis N. Recurrent losses and rapid evolution of the condensin II complex in insects. Mol Biol Evol. 2019 Jul 4;

80. Metz CW. Chromosome studies on the Diptera. II. The paired association of chromosomes in the Diptera, and its significance. Journal of Experimental Zoology. 1916;21(2):213–79.

81. Williams BR, Bateman JR, Novikov ND, Wu C-T. Disruption of topoisomerase II perturbs pairing in drosophila cell culture. Genetics. 2007 Sep;177(1):31–46.

82. Wolfe SL, John B. The organization and ultrastructure of male meiotic chromosomes in oncopeltus fasciatus. Chromosoma. 1965 Jun 1;17(2):85–103.

83. Pe´rez R, Panzera F, Page J, Suja JA, Rufas JS. Meiotic behaviour of holocentric chromosomes: orientation and segregation of autosomes in Triatoma infestans (Heteroptera). Chromosome Res. 1997 Feb 1;5(1):47–56.

84. Moffitt JR, Zhuang X. RNA Imaging with Multiplexed Error Robust Fluorescence in situ Hybridization. Methods Enzymol. 2016;572:1–49.

Supplemental Figures

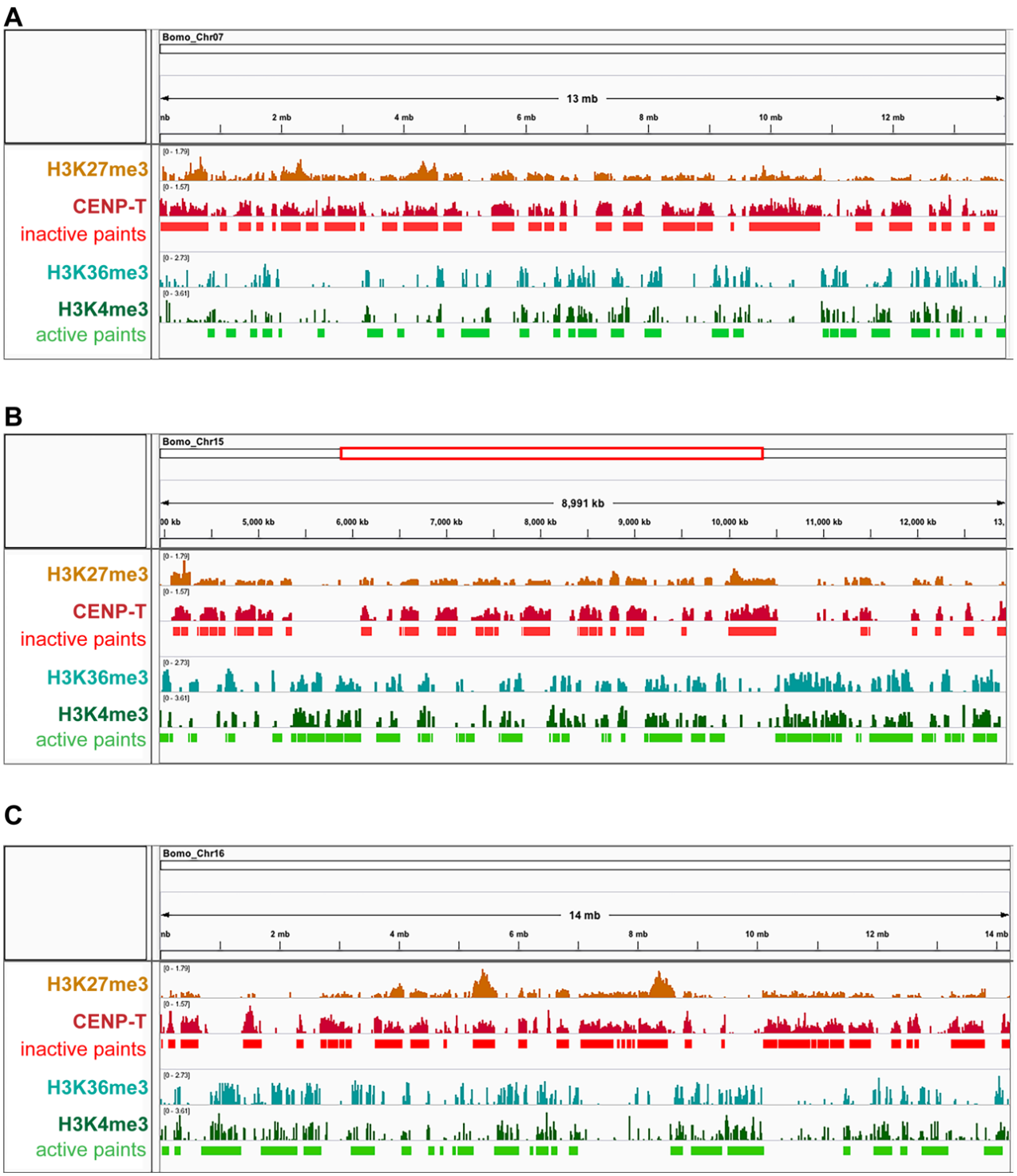

Figure S1. ChIP-seq profiles used to design active and inactive chromosome paints. Screenshots of ChIP-seq data used to design active/inactive chromosome paints. Inactive: H3K27me3 (orange), Centromere Protein T (CENP-T; dark red). Inactive paint domains shown in bright red. Active: H3K36me3 (teal), H3K4me3 (dark green). Active paint domains shown in bright green. ChIP-seq data were previously published (see Materials and Methods). Chromosome 7 is shown in A, part of chromosome 15 is shown in B (coordinates Chr15:3,900,000-12,891,000), and chromosome 16 is shown in C.

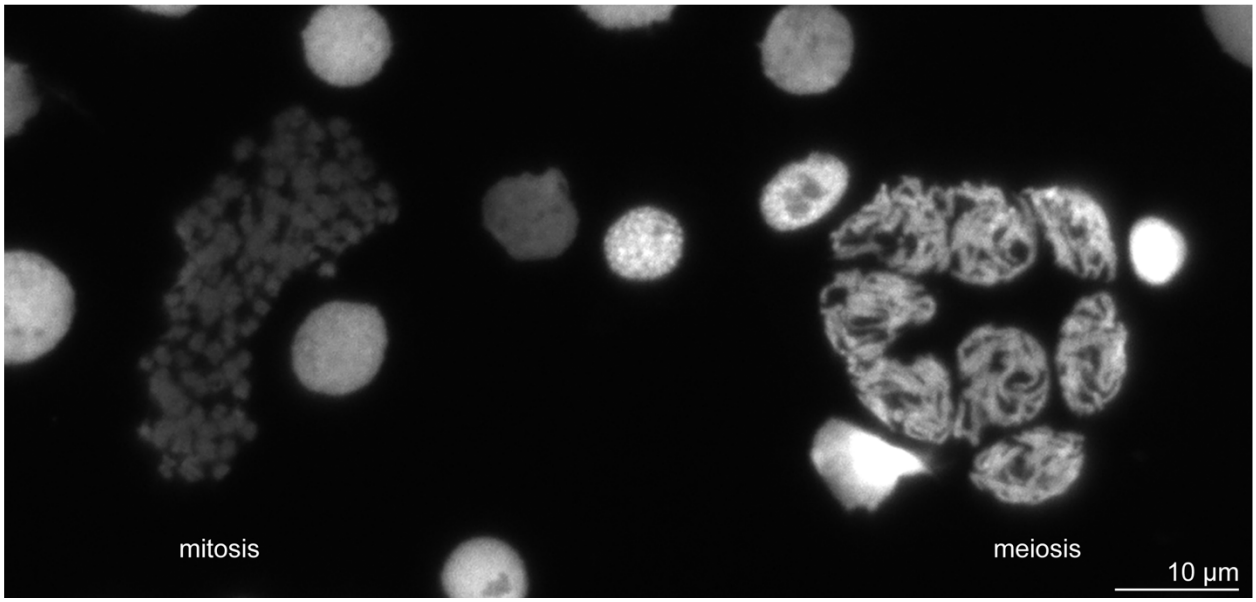

Figure S2. Mitotic and meiotic nuclei in early 5th instar larval testes squash.
Representative image showing a cluster of mitotic chromosomes (left) and a cluster of meiotic prophase I cells (right) labeled with DAPI.

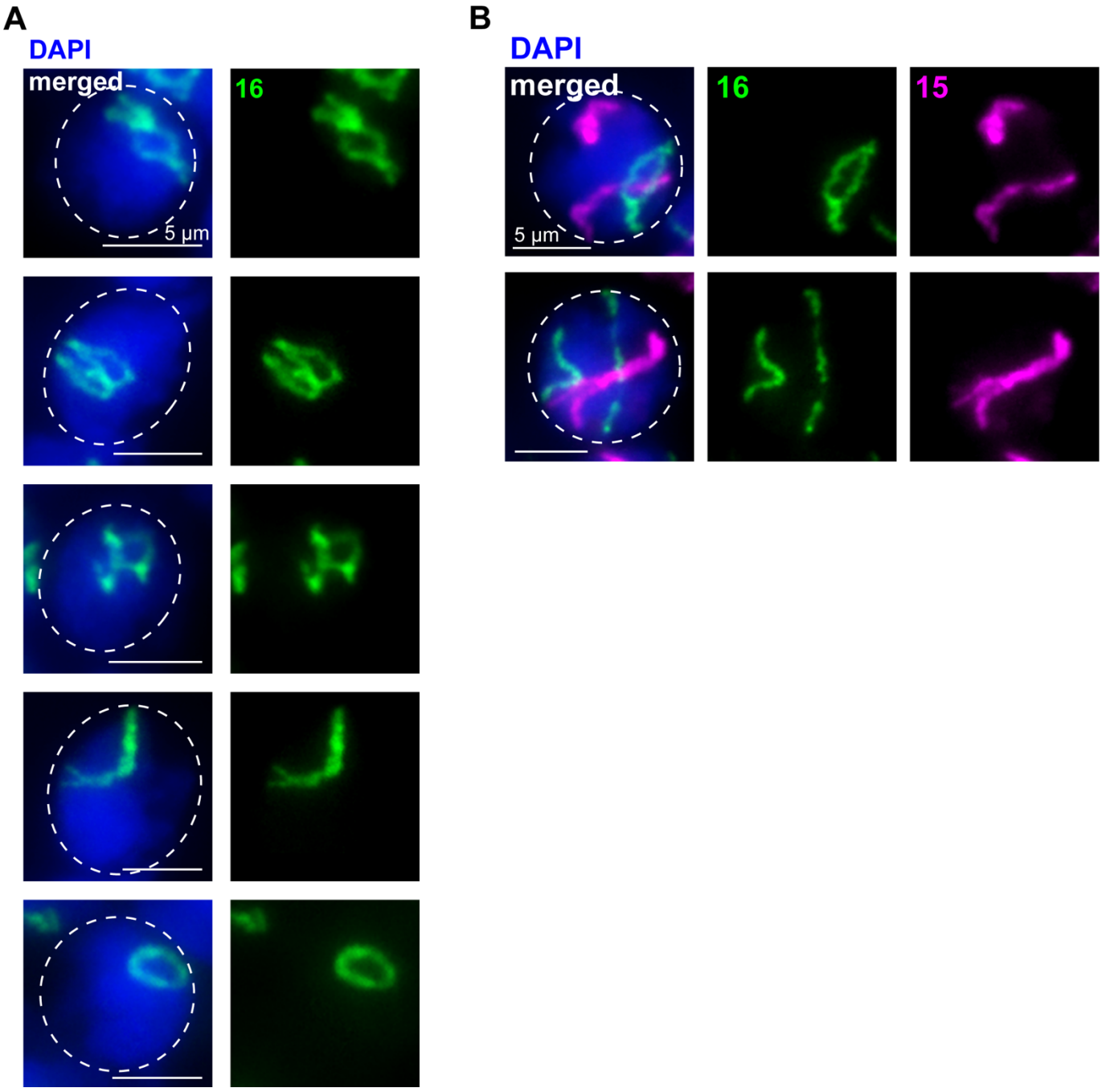

Figure S3. Partially paired chromosome configurations in early meiotic prophase in larval testes.
A) Oligopaints for chromosome 16 (green) in representative zygotene nuclei. Dashed line approximates the nuclear edge.
B) Oligopaints for chromosomes 16 (green) and 15 (magenta) in representative zygotene nuclei. Top: Ch16 has begun pairing while ch15 remains entirely unpaired. Bottom: Ch15 is nearly completely paired while ch16 remains unpaired. Dashed line approximates the nuclear edge.

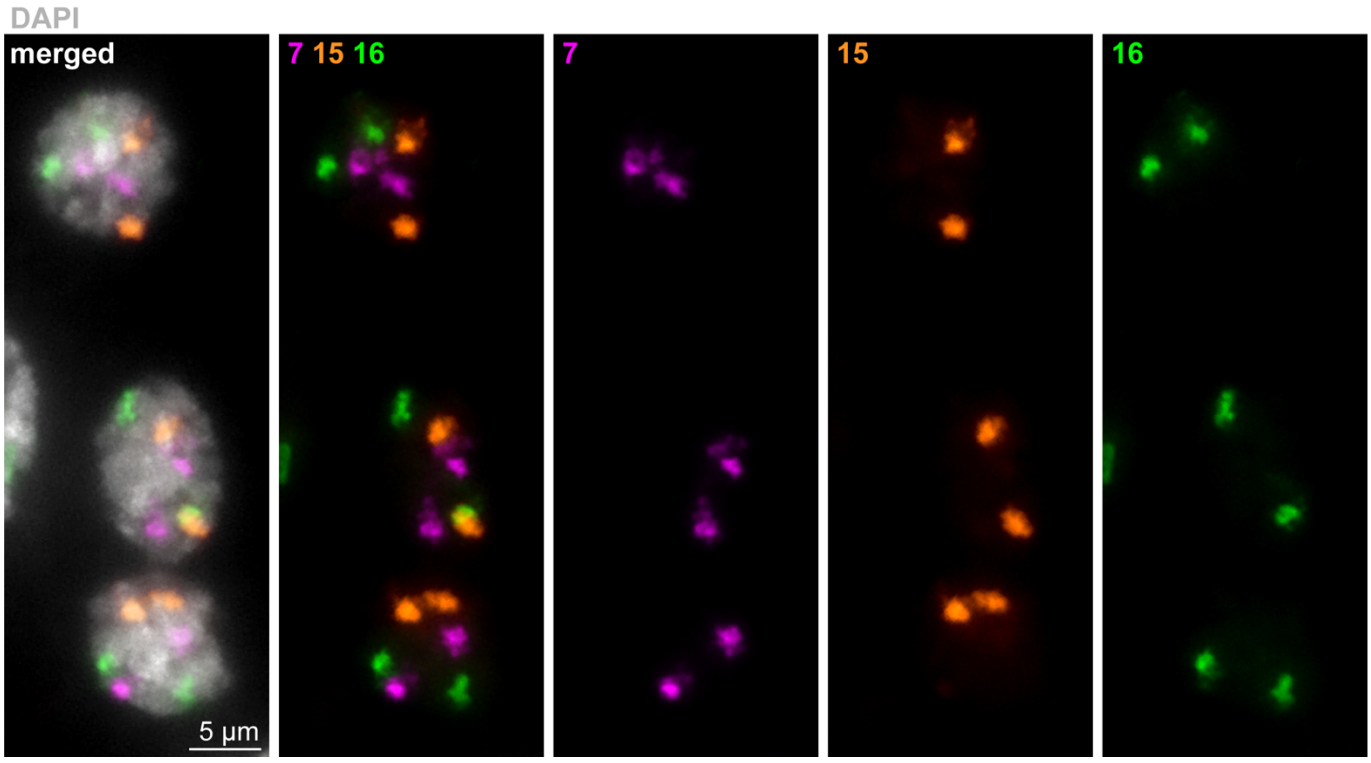

Figure S4. Somatic cells with unpaired homologs from larval testes squashes.
Three nuclei (DAPI in gray) labeled with Oligopaints to chromosomes 7 (magenta), 15 (orange), and 16 (green) in somatic cells from late 4th instar larval testes squash. Two signals per nucleus indicates unpaired homologs.

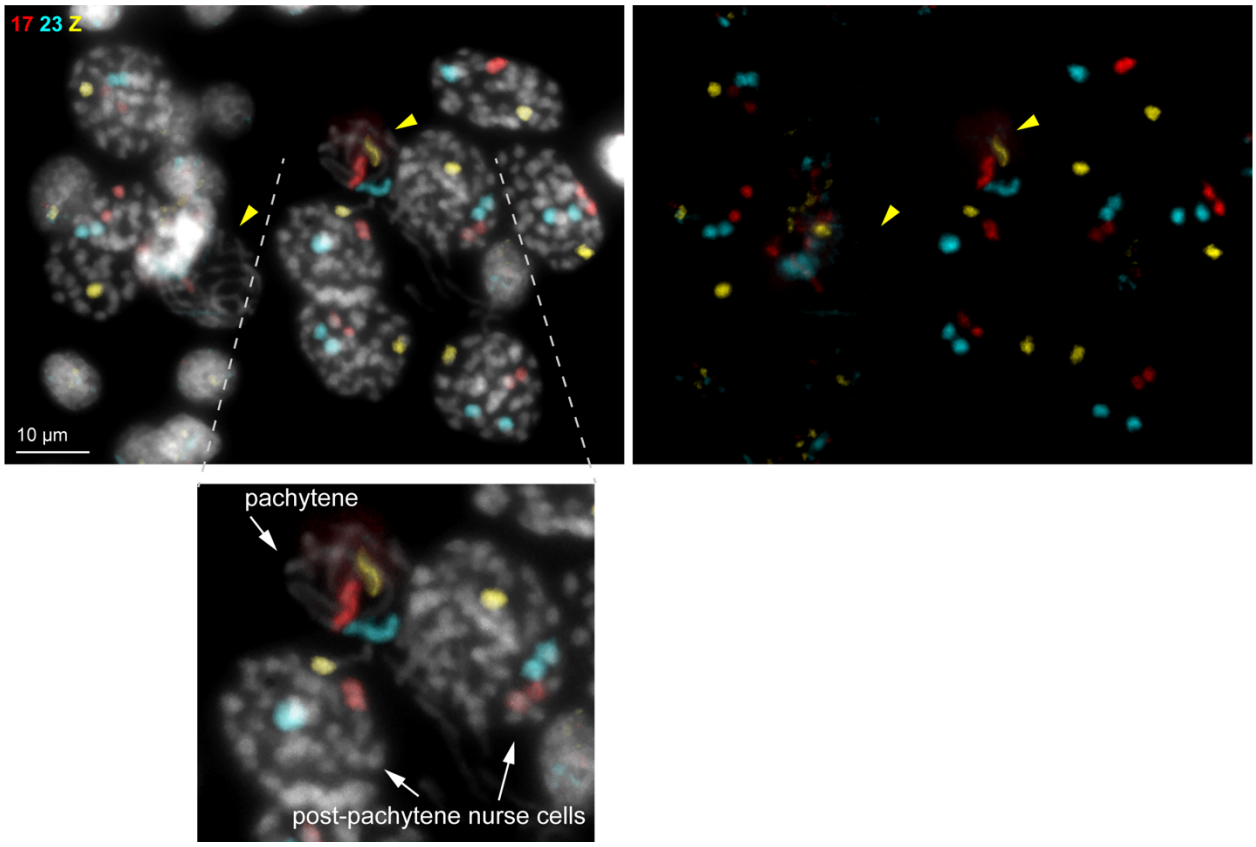

Figure S5. Pachytene and post-pachytene nurse cells labeled with whole chromosome paints.
Top: Representative field from early 5th instar larval ovary squash labeled with whole chromosome paints for ch17 (red), ch23 (cyan), and chZ (yellow). Left, merged with DAPI, right, paints alone. Yellow arrowheads indicate pachytene cells. Note: female *B. mori* are heterogametic and harbor a single Z and a single W chromosome (compared to two copies of ch17 and ch23). As the W chromosome is largely repetitive, it is not suitable for the Oligopaint design utilized here. Bottom: zoom showing pachytene and post-pachytene nurse cells, as indicated.

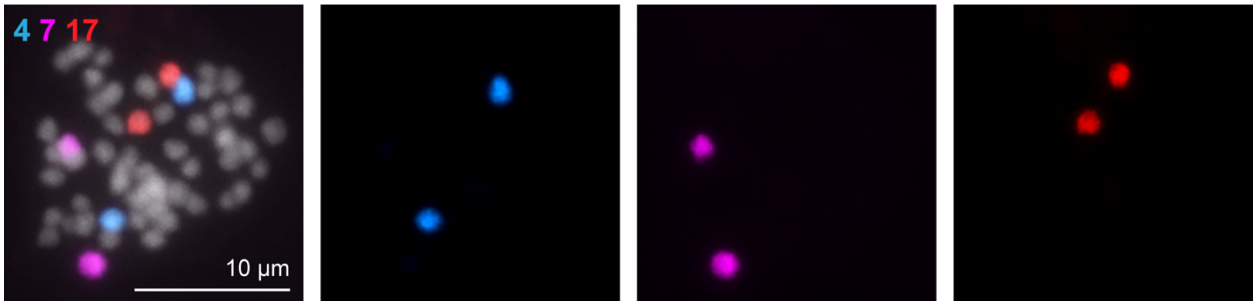

Figure S6. Mitotic cell labeled with whole chromosome paints from 5th instar larval testes.
Representative mitotic cell labeled with whole chromosome paints for ch4 (blue), ch7 (magenta) and ch17 (red).

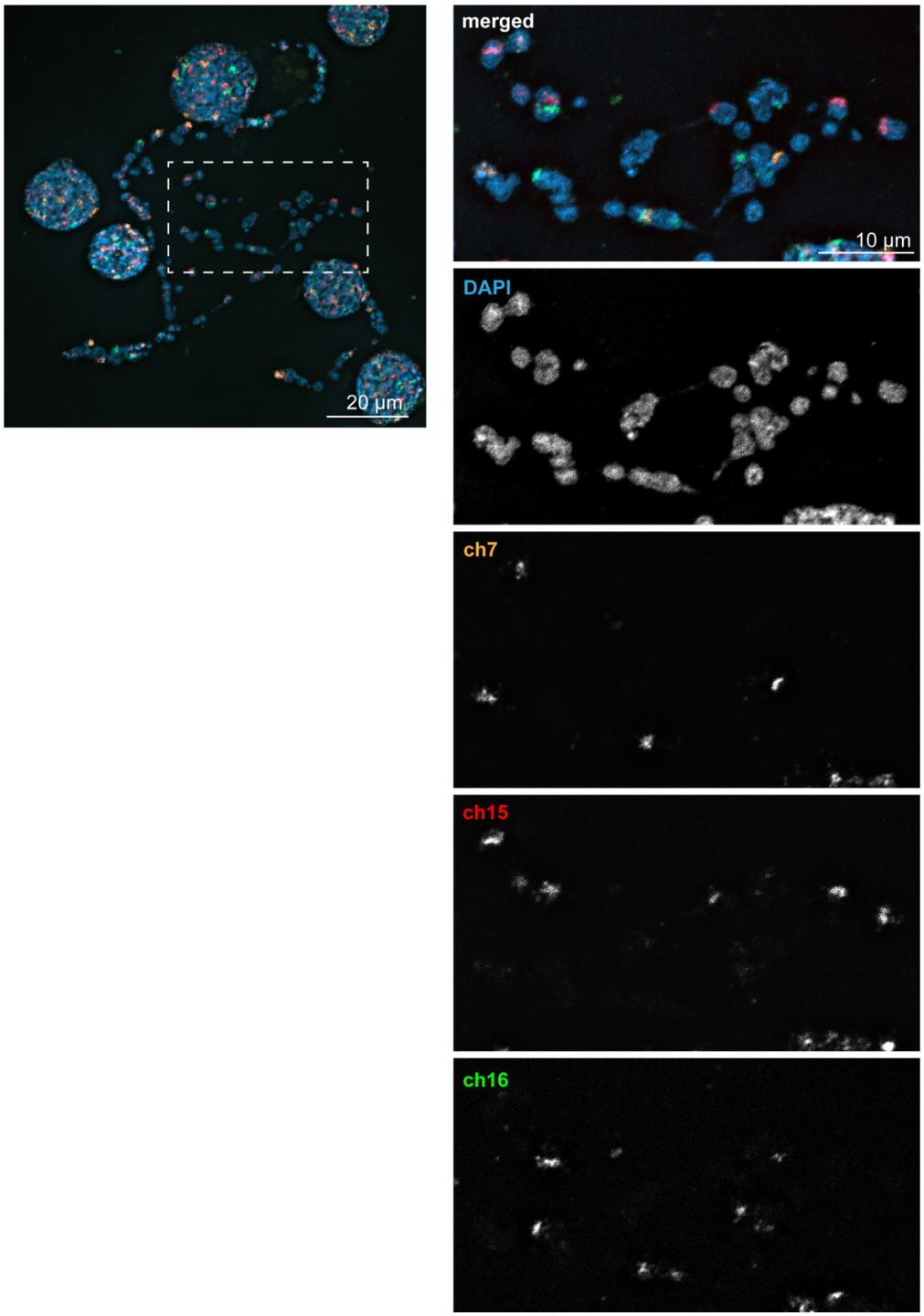

Figure S7. Mitotic spreads from BmN4 cultured cells labeled with whole chromosome Oligopaints. Left: representative mitotic chromosome spread from BmN4 cultured cells labeled with whole chromosome paints for ch7 (orange), ch15 (red), and ch16 (green). White box indicates zoom shown to the right. No entire chromosomes are labeled in the cell line and instead several chromosomes are partially labeled with each paint, indicating a large amount of translocations in the this cell line compared to animals.

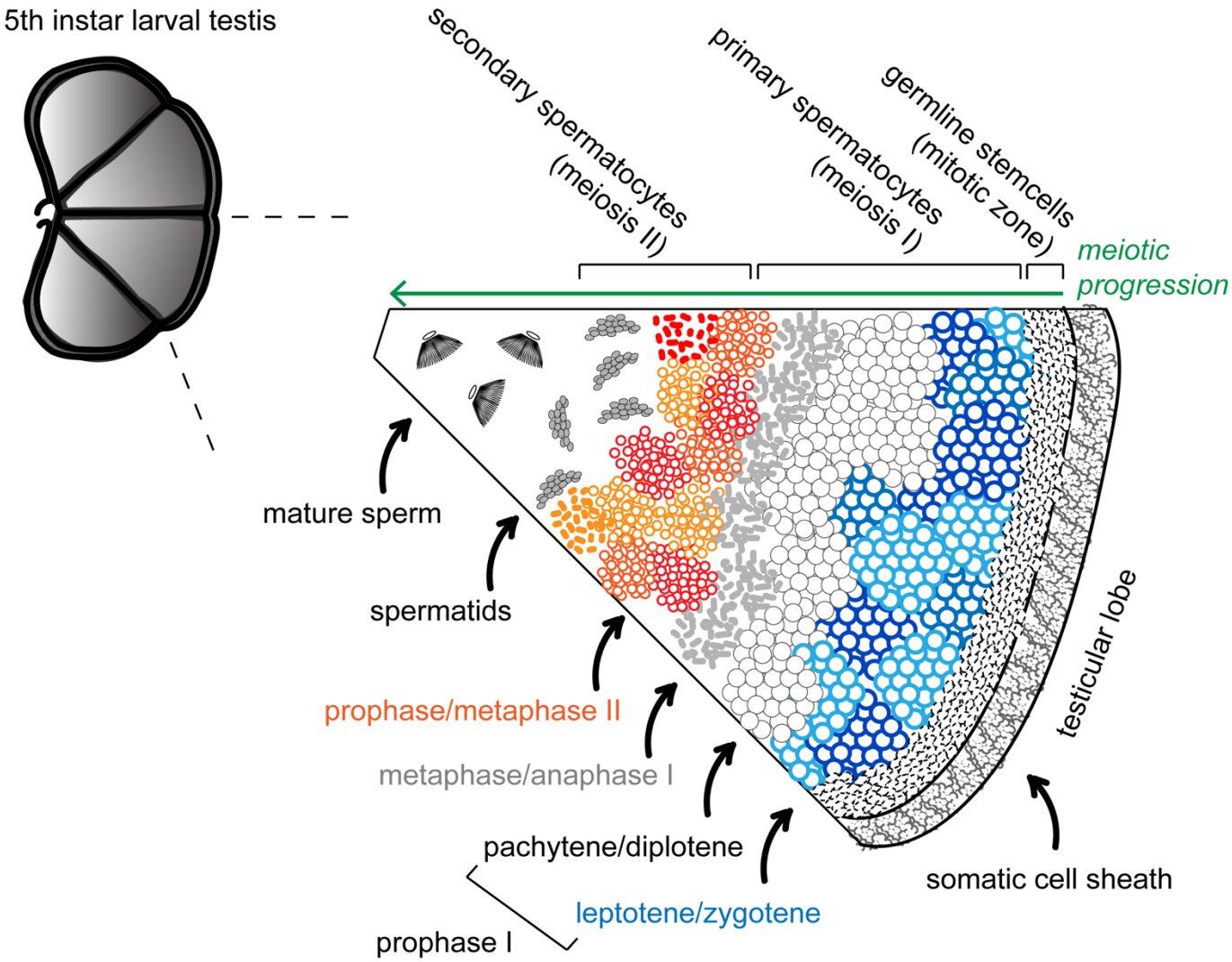

Figure S8. Cartoon schematic of 5th instar larval testis.
Mature 5th instar larval testes are comprised of four testicular lobes, each of which harbors germline stem cells (mitotic zone) and spermatocytes in all stages of meiosis up to mature sperm; progressing from right to left in the image. Additionally, each lobe is surrounded by somatic cells in the sheath and in the septae separating the lobes.

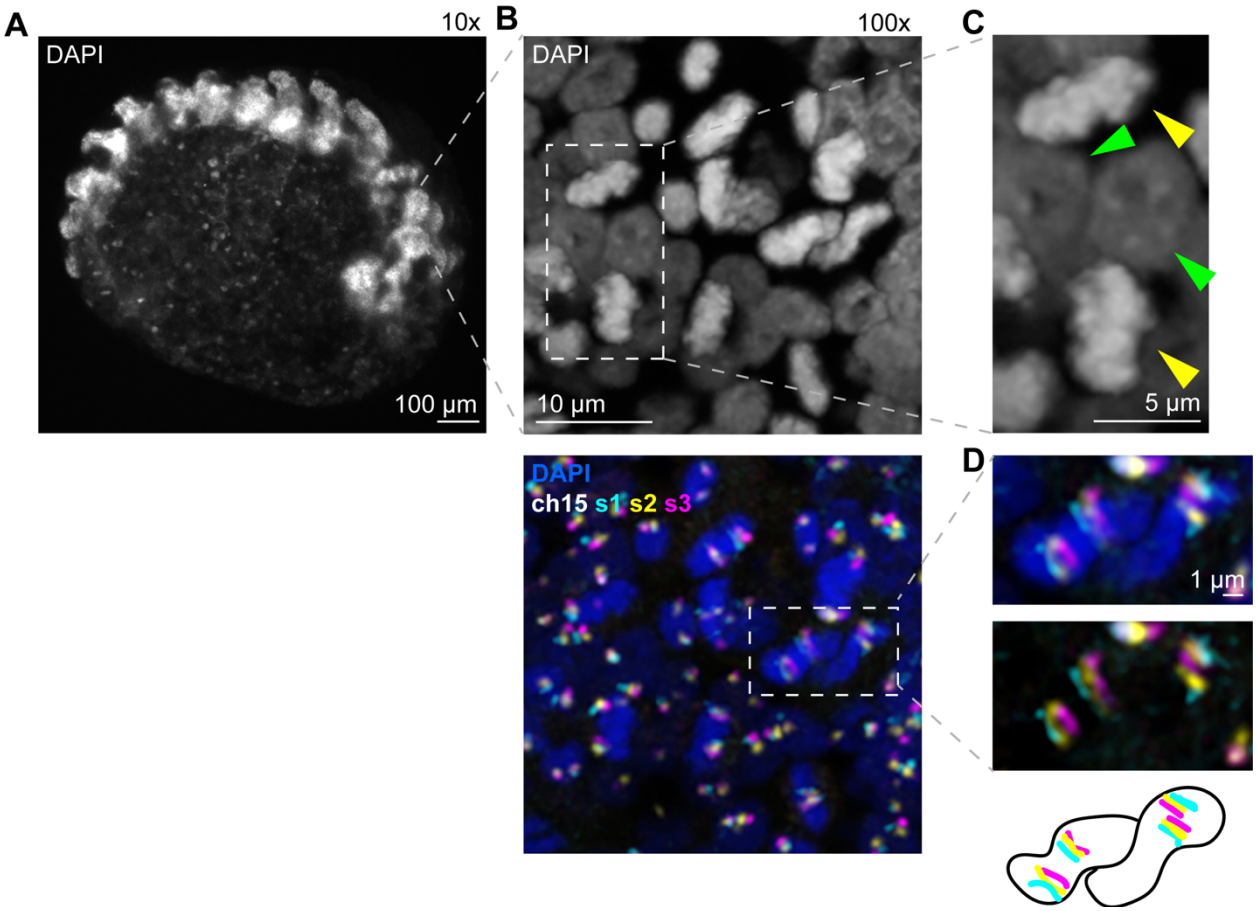

Figure S9. Ch15 stripe paints in a post-diapause embryo.

A) Whole-mount embryo stained with DAPI imaged at 10x.

B) 100x image of whole-mount embryo stained with DAPI (top) and labeled with ch15 stripe paints (bottom).

C) Zoom of B (top). Yellow arrow heads indicate mitotic cells, green arrow heads indicate interphase cells.

D) Zoom of B (bottom), showing two mitotic cells labeled with ch15 stripe paints and DAPI stain (top) or only stripe paints (middle). Bottom, cartoon schematic, with the black outline representing the border of the DAPI stain.

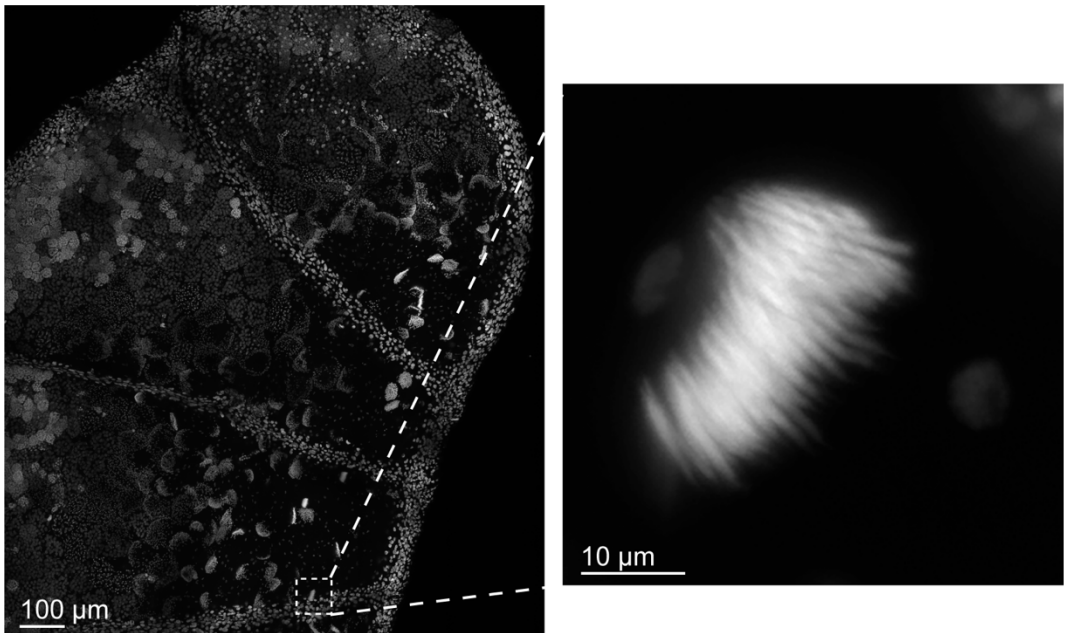

Figure S10. Mature sperm in 5th instar larval testes.
Left: 10x image of larval testes stained with DAPI. White box indicates zoom shown to the right. Right: zoom of mature eupyrene sperm bundle labeled with DAPI.

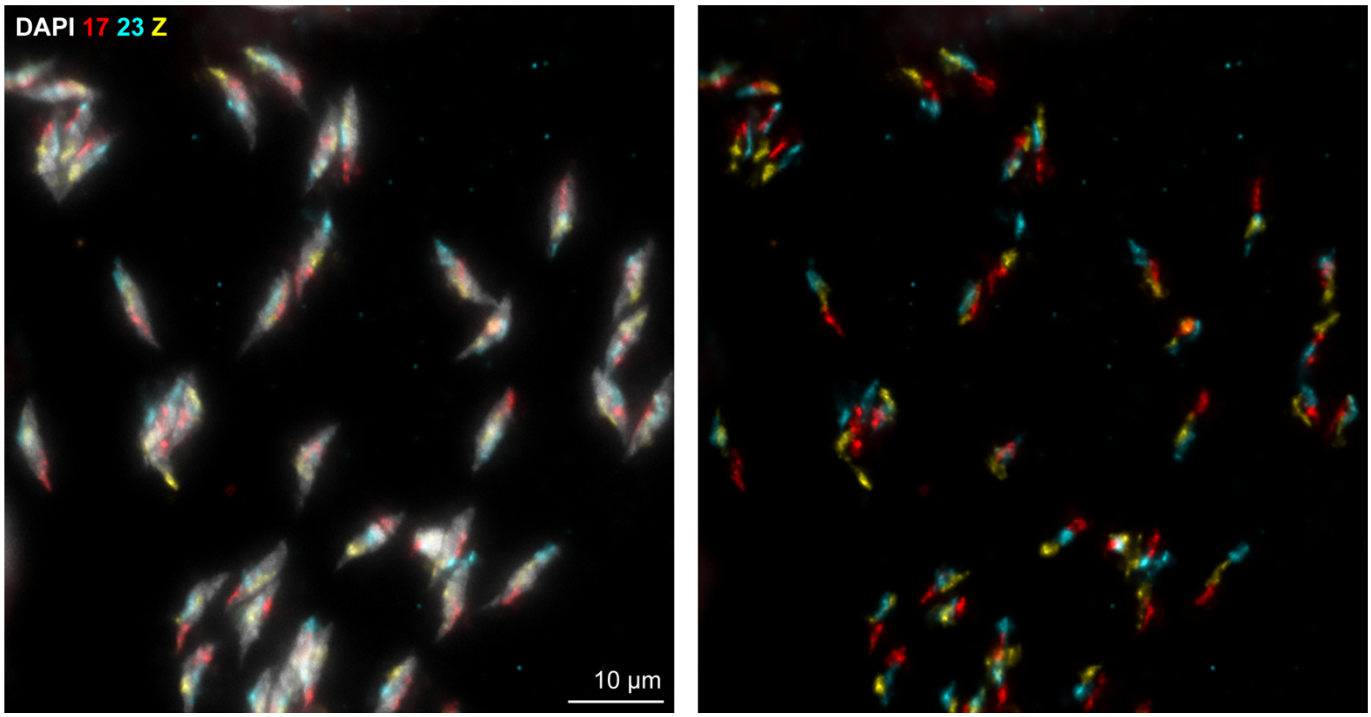

Figure S11. Oligopaints in mature sperm from 5th instar larval testis squash.
Oligopaints labeling chromosomes 17 (red), 23 (cyan) and Z (yellow) in mature sperm from a 5th instar larval testis squash. DAPI is shown in gray.

Figure S12. 5th instar larval ovary.
DAPI staining on a whole mount 5th instar larval ovary.